

Fall 2009

Thermal Modeling of Lithium-Ion Energy Storage Systems for Hybrid Electric Vehicles Using Computational Fluid Dynamics with Conjugate Heat Transfer

Craig R. Czapinski
Embry-Riddle Aeronautical University - Daytona Beach

Follow this and additional works at: <https://commons.erau.edu/db-theses>



Part of the [Mechanical Engineering Commons](#)

Scholarly Commons Citation

Czapinski, Craig R., "Thermal Modeling of Lithium-Ion Energy Storage Systems for Hybrid Electric Vehicles Using Computational Fluid Dynamics with Conjugate Heat Transfer" (2009). *Theses - Daytona Beach*. 37.

<https://commons.erau.edu/db-theses/37>

This thesis is brought to you for free and open access by Embry-Riddle Aeronautical University – Daytona Beach at ERAU Scholarly Commons. It has been accepted for inclusion in the Theses - Daytona Beach collection by an authorized administrator of ERAU Scholarly Commons. For more information, please contact commons@erau.edu.

THERMAL MODELING OF LITHIUM-ION ENERGY STORAGE SYSTEMS FOR
HYBRID ELECTRIC VEHICLES USING COMPUTATIONAL FLUID
DYNAMICS WITH CONJUGATE HEAT TRANSFER

By

Craig R. Czapinski

A Thesis Submitted to the

Graduate Studies Office

In Partial Fulfillment of the Requirements for the Degree of
Masters of Science in Mechanical Engineering

Embry-Riddle Aeronautical University

Daytona Beach, Florida

Fall 2009

UMI Number: EP31985

INFORMATION TO USERS

The quality of this reproduction is dependent upon the quality of the copy submitted. Broken or indistinct print, colored or poor quality illustrations and photographs, print bleed-through, substandard margins, and improper alignment can adversely affect reproduction.

In the unlikely event that the author did not send a complete manuscript and there are missing pages, these will be noted. Also, if unauthorized copyright material had to be removed, a note will indicate the deletion.

UMI[®]

UMI Microform EP31985
Copyright 2011 by ProQuest LLC
All rights reserved. This microform edition is protected against
unauthorized copying under Title 17, United States Code.

ProQuest LLC
789 East Eisenhower Parkway
P.O. Box 1346
Ann Arbor, MI 48106-1346

Copyright by Craig R. Czapinski
All Rights Reserved

THERMAL MODELING OF LITHIUM-ION ENERGY STORAGE SYSTEMS FOR
HYBRID ELECTRIC VEHICLES USING COMPUTATIONAL FLUID
DYNAMICS WITH CONJUGATE HEAT TRANSFER

by

Craig R. Czapinski

This thesis was prepared under the direction of the candidate's thesis committee chairman, Dr. Darris White, Department of Mechanical Engineering, and has been approved by the members of his thesis committee. It was submitted to the Mechanical Engineering Department and was accepted in partial fulfillment of the requirements for the degree of Masters of Science in Mechanical Engineering.

THESIS COMMITTEE:



Dr. Darris White
Chairman



Dr. William Barott
Member



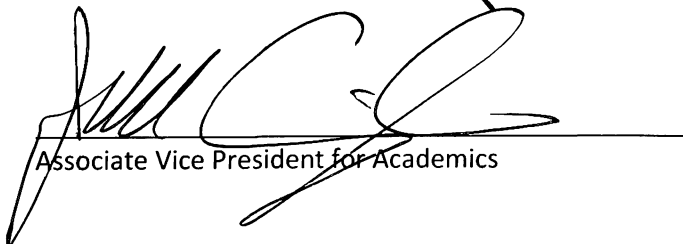
Professor J.E. McKisson
Member



Department Chair, Mechanical Engineering

11/23/09

Date



Associate Vice President for Academics

12/17/09

Date

ACKNOWLEDGEMENTS

This thesis would not have been possible without the guidance from my thesis committee. Their help along with the resources of the Embry-Riddle EcoEagles Team were crucial to the successful completion of this thesis. I would also like to thank my friends for their assistance and for providing occasional amusement. Finally, I thank my parents for supporting me throughout all my studies at Embry-Riddle Aeronautical University.



ABSTRACT

Author: Craig R. Czapinski
Title: Thermal Modeling Of Lithium-Ion Energy Storage Systems For Hybrid Electric Vehicles Using Computational Fluid Dynamics With Conjugate Heat Transfer
Institution: Embry-Riddle Aeronautical University
Degree: Master's of Science in Mechanical Engineering
Year: 2009

The success and performance of a Hybrid Electric Vehicle (HEV) relies largely on its Energy Storage System (ESS). High temperatures and thermal variations can significantly affect a battery's performance and lifecycle. An effective thermal management system is vital to the health and safe operation of the ESS's batteries. A well designed thermal management system begins with the accurate prediction of the battery's thermal conditions. In hot climates, HEVs may be required to operate within ten degrees Celsius of the maximum safe operating temperature of their batteries. This study aims to evaluate the thermal management system of a lithium-ion based energy storage system designed for HEV applications. The analysis uses estimated current values from powertrain simulation software, fundamental heat transfer principles, finite element analysis (FEA), and computational fluid dynamics (CFD) tools to predict the temperature distributions in battery modules.

TABLE OF CONTENTS

ACKNOWLEDGEMENTS.....	iv
ABSTRACT.....	v
LIST OF TABLES.....	viii
LIST OF FIGURES.....	ix
LIST OF ACRONYMS.....	xi
CHAPTER 1: INTRODUCTION.....	1
Background.....	1
EcoCAR The NeXt Challenge.....	4
ESS Design Requirements and Procedure.....	6
Research Objectives.....	7
Outline.....	7
CHAPTER 2: METHOD.....	8
A123® Li-Ion Batteries.....	8
Energy Storage System.....	13
Electrical Modeling and Simulation.....	15
Heat Production in Battery Modules.....	18
Software: SolidWorks® 2009 Flow Simulation.....	19
Assumptions.....	23
CHAPTER 3: ANALYSIS.....	24
Cold Plate Design and Analysis.....	24
Cold Plate Analysis Summary.....	30
Fluid Path Design and Analysis.....	32
Heat Exchanger Analysis Summary.....	38
Coolant Pressure Calculations.....	39
Sensitivity Analysis.....	42

CHAPTER 4: CONCLUSION.....	46
Summary of Analysis.....	46
Variations in Ambient Temperature	47
ESS Assembly	48
System Limitations.....	51
CHAPTER 5: RECOMMENDATIONS.....	52
Analysis Limitations	52
Future Research: Time Dependent Analysis	53
Future Research: Heat Soaked ESS	53
REFERENCES.....	54
APENDIX A: A123 Prismatic Module Drawings	58

LIST OF TABLES

Table 1: Battery Systems (7)	2
Table 2: A123® Prismatic Cell Properties (19).....	9
Table 3: 25S2P Module Properties (19)	11
Table 4: Thermal Properties of Aluminum 6061 (23) (24).....	14
Table 5: PSAT ESS - Load Simulation Data (26)	17
Table 6: Cooling System Properties	25
Table 7: Cold Plate Solver Parameters.....	31
Table 8: Cold Plate Solver Goal Parameters	31
Table 9: Fluidyne® Heat Exchanger Model Properties.....	34
Table 10: SPAL Fan Airflow at 13V (42).....	35
Table 11: Heat Exchanger Solver Parameters.....	38
Table 12: Heat Exchanger Solver Goal Parameters	38
Table 13: Coolant Path Properties	40
Table 14: Dedenbear WP3 Water Pump Specifications (45)	41
Table 15: Fluid Flow Rates vs. ΔT	42

LIST OF FIGURES

Figure 1: EcoCAR Saturn® Vue® (15).....	4
Figure 2: EcoCAR Boston Workshop (16).....	5
Figure 3: A123® 20Ah Lithium-Ion Prismatic Cell (18).....	8
Figure 4: DC Resistance Temperature Dependence (19).....	10
Figure 5: A123® 25S2P Prismatic Module (19).....	10
Figure 6: A123® 25S2P Prismatic Module Exploded View (19).....	11
Figure 7: SolidWorks® Model of 25S2P Module.....	12
Figure 8: SolidWorks® Model of Thermal Mass.....	12
Figure 9: Prismatic Cell with Heat Sink Foil (19).....	12
Figure 10: Prismatic Cells with Heat Sink Foil Interleaved Between Every Other Cell (19).....	12
Figure 11: ESS Installed In Saturn® Vue® (21).....	13
Figure 12: Side View of ESS Installed In Saturn® Vue® (22).....	13
Figure 13: EcoEagles Powertrain Configuration (14).....	15
Figure 14: FTP-72 Urban Dynamometer Driving Schedule (27).....	16
Figure 15: EPA Highway Fuel Economy Cycle (28).....	16
Figure 16: Specific Heat of Aluminum (34).....	20
Figure 17: Specific Heat of Water (35).....	20
Figure 18: Simplified CAD Model of Cold Plate and Battery Modules.....	25
Figure 19: Flow Trace of Coolant through Cold Plate Showing Coolant Temperature.....	26
Figure 20: Surface Temperature of Cold Plate (Top View).....	27
Figure 21: Surface Temperature of Cold Plate with Coolant Flow Traces (Bottom View).....	27
Figure 22: Center Temperature of ESS (Front View).....	28
Figure 23: Surface Temperature of ESS.....	28
Figure 24: Flow Trace Through Cold Plate Showing Coolant Pressure.....	29
Figure 25: Cold Plate Boundary Conditions and Heat Sources.....	30
Figure 26: Coolant Paths (40).....	32
Figure 27: Fluidyne® DB-30618 Heat Exchanger (533 x 150 x 76 mm) (41).....	33
Figure 28: Fluidyne® Heat Exchanger Simplified CAD Model.....	33
Figure 29: SPAL VA67-A101-83A Fan (42).....	34
Figure 30: Fluid Pressure along Heat Exchanger Core Centerline.....	35
Figure 31: Flow Trace over Heat Exchanger Core Showing Air Temperature.....	36

Figure 32: Surface Temperature of Heat Exchanger Core	37
Figure 33: Fluid Temperature along Heat Exchanger Core Centerline	37
Figure 34: Fluidyne® Heat Exchanger Performance (44)	40
Figure 35: Dedenbear WP3 Water Pump (45)	41
Figure 36: Water Temperature Change Chart (47)	43
Figure 37: 50% Ethylene Glycol and Water Temperature Change Chart (47)	44
Figure 38: Air Temperature Change Chart (47).....	45
Figure 39: Exploded ESS Component Assembly (26)	48
Figure 40: Finished Structural Cold Plate.....	49
Figure 41: Finished Structural Cold Plate with A123® 25S2P Module Mock Ups	49
Figure 42: ESS Assembly (26)	50
Figure 43: Battery Pack Location Outside of Rear Crush Zone (26).....	50
Figure 44: Major Dimensions of ESS in mm (26).....	51

LIST OF ACRONYMS

BCM: Battery Control Module

CAD: Computer Aided Design

CFD: Computational Fluid Dynamics

DCR: Direct Current Resistance

DOE: Department of Energy

EDS: Emergency Disconnect System

EGW: Ethylene Glycol and Water

eRDM: Electric Rear Wheel Drive System

ESS: Energy Storage System

EV: Electric Vehicle

FEA: Finite Element Analysis

HEV: Hybrid Electric Vehicle

HV: High Voltage

HWFET: Highway Fuel Economy Test

HyREV: Hybrid and extended-Range Electric Vehicle

ICE: Internal Combustion Engine

Li-Ion: Lithium Ion

MPGGE: Miles Per Gallon Gasoline Equivalent

MSD: Manual Service Disconnect

NiMH: Nickel Metal Hydride

PSAT: Powertrain Systems Analysis Toolkit

RAM: Random Access Memory

RMS: Root Mean Square

RPIM: Rear Power Inverter Module

SOC: State of Charge

TPIM: Transmission Power Inverter Module

UDDS: Urban Dynamometer Driving Cycle

WTW: Well-To-Wheel

CHAPTER 1: INTRODUCTION

This chapter provides background information on the research that was conducted throughout the course of this study. Information on prior research of batteries for Hybrid Electric Vehicles (HEVs) and Electric Vehicles (EVs) is also presented. An introduction is given on the objectives of this research and its importance. Additionally, an overview of the study that was conducted and its presentation are provided.

Background

The performance of HEVs relies heavily on their Energy Storage System (ESS). Unlike EV batteries, which are intended for high capacity, relatively constant low to moderate discharge rates, HEV batteries are designed for many high power charge cycles (1). The battery performance requirements of HEVs are as follows (2)(3):

1. High specific energy density
2. High volumetric energy density
3. High power density
4. Easy charging management
5. High cycle life
6. Long calendar life
7. Stable performance at low temperatures

There are two classes of batteries for HEVs: power assist and dual mode. Power assist are small in size and capacity compared to dual mode batteries which are used for hybrid drive or electric drive (4). Both of these classes tend to have high discharge rates relative to their energy storage capacity. The high power charges and discharges cause the battery's temperature to rise due to ohmic heating. Temperature gradients caused by uneven cooling present problems in most battery types. These gradients can affect the utilization of active material in the cell, with the

warmer regions being more active than the cooler regions (5). Also, batteries generally have a higher degradation rate at high temperatures which can significantly reduce the life of the batteries (6).

There are several types of batteries available for HEVs. The three most common types are lead, nickel, and lithium systems. The following table lists several of the properties of each aforementioned type.

Table 1: Battery Systems (7)

Properties	Lead-Acid System open/sealed	Nickel Systems Nickel-cadmium Nickel-metal hydride	Lithium Systems Lithium-ion Lithium-polymer
Cell Voltage	2 V	1.2 V	3...4 V
Energy density	25...30 Wh/kg	35...80 Wh/kg	60...150 Wh/kg
Energy efficiency without heating/cooling	75...80%	60...85%	85...90%
Power density	100.200 W/kg	100...1,000 W/kg	300...1,500 W/kg
Service life in cycles	600...900	> 2,000	> 1,000 projected
Operating temperature	10...55 °C	-20...55 °C	-10...50 or 60 °C
Maintenance free	Depending on design	Depending on design	Yes

Lithium-ion batteries offer advantages in energy density, power density, and cost over other available technologies (8). However, lithium-ion batteries are sensitive to overheating and for this reason, lithium-ion batteries have yet to replace NiMH as the battery of choice in the HEV market (9). Even though each battery type's reaction to high temperatures varies, maintaining optimum, uniform temperature or some method of thermal management is essential to obtain peak battery performance for all types (10). Liquid or air cooling is commonly used to control the temperature of the batteries. Cooling systems are not the only method for regulating battery temperatures. A battery controller can prevent excessive temperatures in the batteries by limiting the allowable current as the temperature of the batteries rise (6).

Nickel metal-hydrate batteries, although the current battery of choice in industry, aren't without a notable thermal disadvantage. The charge efficiency of NiMH batteries declines at temperatures above 35 °C. This effect creates a "vicious circle" where the temperature of the battery climbs further due to the reduced efficiency. Lithium-ion batteries do not display such a characteristic because they have a coulomb efficiency of nearly 100%. Also, the newest versions of Li-Ion batteries have lower internal resistance than most batteries. Their low resistance combined with nearly 100% coulomb efficiency causes Li-ion batteries to produce less heat for a given power than other battery types (11).

Apart from the catastrophic effects of temperature on energy storage systems, maintaining uniform temperatures within the individual cells affects both the battery life and performance of the HEV. Variations in battery temperature may be due to inconsistent impedance, non-uniform thermal characteristics, and the effects of high ambient temperature (10). Variations in temperature also affect the charge termination voltage of the cells. The use of a temperature compensated charging system is necessary to fully utilize the batteries (12).

For lithium-ion batteries, charging is an endothermic reaction. When charging under 0.5C, the heat absorbed is greater than the ohmic heat produced from the battery's internal resistance. This leads to drops in battery temperature during low current charging. Therefore, regulating the charge cycle could absorb a portion of the heat produced due to vehicle operation (6).

The successful implementation and commercialization of HEVs rely largely on energy storage systems. Lithium-ion batteries are considered the only viable energy storage device for HEV applications. Although lithium-ion batteries have been widely used in electronics devices, they

are not yet ready for commercial use in HEVs due to the thermal limitations (13). A successful thermal management system starts with accurate prediction of the thermal conditions of the battery. This study is aimed to evaluate the thermal management system of a lithium-ion battery pack designed for HEV applications.

EcoCAR The NeXt Challenge

The EcoCAR challenge is an effort by the US Department of Energy (DOE), General Motors, and National Resources Canada to promote the development of cleaner, more efficient vehicles as part of a comprehensive educational program. The EcoEagles team represents Embry-Riddle Aeronautical University in this three year competition. The design goals for this competition are to reduce petroleum energy consumption and reduce well-to-wheel (WTW) emissions, while maintaining consumer acceptability. Due to the availability and efficiency of electricity and electric power systems, vehicle electrification was identified as a key technology for this project (14).



Figure 1: EcoCAR Saturn® Vue® (15)

"The Embry-Riddle HyREV system is an innovative combination of power split **Hybrid** and extended-**Range Electric Vehicle** technologies, designed to reduce petroleum energy consumption and improve vehicle efficiency across a range of operating conditions. The HyREV system was developed for the EcoCAR Challenge and is capable of full function electric operation for approximately 32 *km* (20 miles). The HyREV design incorporates an efficient 1.3-liter diesel engine, using B20 biodiesel fuel, with the electric motors in the General Motors (GM) Two-Mode Transmission and Magna eRDM to create a propulsion system capable of a combined fuel economy of approximately 40 *mpgge* on the Saturn® Vue® platform" (14).



Figure 2: EcoCAR Boston Workshop (16)

The thermal management system that is the focus of this study will be implemented on EcoEagles vehicle entry for the EcoCAR Challenge. As part of the competition, the vehicle will be tested in extreme conditions to evaluate the design. Therefore, the analysis in this study is aimed to simulate these conditions. Because the results of this study will be applied to the design of the EcoEagles vehicle there will be an opportunity to compare the results of this study to the performance of the actual design.

ESS Design Requirements and Procedure

The following describes the requirements of the thermal management system as well as the procedure used to ensure the requirements are met (17):

Step 1: Perform drive cycle analysis. This step examines the current requirements for the battery. The results of this step will be used to estimate the heat production of the batteries in a worst case scenario.

- a. It is necessary to consider the most strenuous drive cycle.
- b. The analysis must consider the basic characteristics of the vehicle that determine energy flow from the batteries:
 - i. Loaded weight of vehicle
 - ii. Drivetrain efficiency
 - iii. Rolling resistance
 - iv. Aerodynamics
- c. Use a Root Mean Square (RMS) method to determine the average effective current.

Step 2: Estimate the heat generation rate. This step determines the power that the thermal management system must be designed to dissipate.

- a. Using an I^2R ohmic heating relationship with the RMS current from step 1, the heat generation will be determined.

Step 3: Analyze the cold plate design. The cold plate must be able to prevent the hottest point of the batteries from reaching 50 °C when the vehicle is subjected to an ambient air temperature of 40 °C. The result of this step is the selection of a cold plate design.

- a. Select a design that will conform to the spatial requirements of the vehicle.
- b. Find necessary coolant flow rate that provides acceptable temperature rise.
 - i. Select a coolant composition that suits the operating conditions.
 - ii. Consider additional thermal resistances imposed by the design.
- c. Attempt to minimize hot spots created by uneven cooling.
- d. Find the coolant pressure drop in the cold plate.

Step 4: Analyze the heat exchanger design. The result of this step should be the selection of a specific heat exchanger model. The analysis must consider high ambient conditions (40 °C).

- a. Select a heat exchanger that can accommodate the flow from step 3.
- b. Determine necessary airflow over the heat exchanger.
- c. Verify the inlet and outlet temperatures match the requirements of the cold plate from step 3.
- d. Find coolant pressure drop in the heat exchanger.
- e. Select a pump using the pressure drop across the entire fluid circuit.
- f. Find the air pressure drop over the heat exchanger.
- g. Select a fan to provide adequate airflow over the heat exchanger.

Research Objectives

The primary goals of this research are to:

1. Select a preliminary cooling system configuration for the EcoEagles ESS based on a towing simulation in a desert environment.
2. Analyze the performance of the cooling system using CFD and thermal finite element software.
3. Perform subsequent design/analysis iterations until a satisfactory design has been achieved.
4. Establish performance limitations of the cooling system configuration.

Outline

Chapter 2 gives an explanation of the characteristics of the batteries used, estimation methods for determining the heat produced within the battery modules, the software used for analysis, and the assumptions made when performing the analysis. Chapter 3 describes the design and the results of the thermal analysis of the ESS for the cold plate and fluid path. Chapter 4 presents the conclusion and explains the significance of the results as they apply to the EcoEagles Vue. Chapter 5 discusses the recommendations for future research and analysis.

CHAPTER 2: METHOD

This chapter describes the Li-Ion cells used in the EcoEagles ESS. Background information will be provided on the battery cell properties as well as the combined properties of the A123[®] 25S2P pack. Simulations that were used to estimate the heat production of the packs are presented. Also included in this chapter is a description of the software used to perform the analysis. Finally, the assumptions made in the analysis are discussed.

A123[®] Li-Ion Batteries

For this application, A123Systems[®] was selected as the supplier of Li-Ion batteries. Figure 3 shows a single A123[®] 20Ah prismatic cell that are stacked to produce prismatic modules for the EcoEagles ESS.

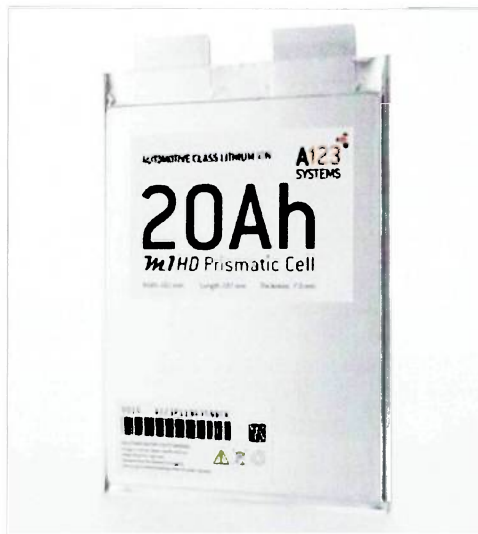


Figure 3: A123[®] 20Ah Lithium-Ion Prismatic Cell (18)

The prismatic cell offers a significant packaging advantage over cylindrical cells. However, the prismatic cells cannot be air-cooled since they are too closely packed with other cells for sufficient airflow to pass between. For this reason it is necessary to implement a liquid cooling system to manage the temperature of the batteries. Reference Table 2 for a list of the relevant thermal properties of the A123[®] 20Ah prismatic cell for analysis.

Table 2: A123® Prismatic Cell Properties (19)

Capacity	19.6 Ah
Nominal Voltage	3.3 V
Nominal Energy	64 Wh
Energy Density	135 Wh/kg, 245 Wh/L
Mass	0.48 kg
Power (@ 25°C, 10 sec, 50% SOC)	650 W
Dimensions	165 x 227 x 7.05 mm
DC Resistance (@ 25°C)	2.4 mΩ
Heat Capacity	480 J/K
R-Value (From Cell to Side Surface)	Side: 2.9 °C/W Bottom: 4.8 °C/W

A123® provides a thermal resistance (R-value) for heat extracted from the bottom or side surfaces of the cells. The overall thermal resistance is characterized by (20):

$$R = \frac{L}{kA}$$

Where:

L = Length of material

k = Thermal conductivity

A = Contact area

Due to the limited space in the rear of the Saturn® Vue®, each of the four A123® batteries is located so that the bottom surface is in contact with the cold plate. Converting the R-value of the bottom surface to thermal conductivity is necessary for simulating the temperature distribution in the battery module. The thermal conductivity of each battery is found using the R-value of the cell's bottom as follows:

$$k = \frac{(0.243 \text{ m})(50 \text{ Cells})}{(4.8 \text{ } ^\circ\text{C}/\text{W})(0.064 \text{ m}^2)} = 39.55 \text{ W}/\text{m K}$$

The DC resistance of the cells is another important property because it is used to estimate the heat produced from charging and discharging. Figure 4 illustrates the temperature dependence of the cell's resistance.

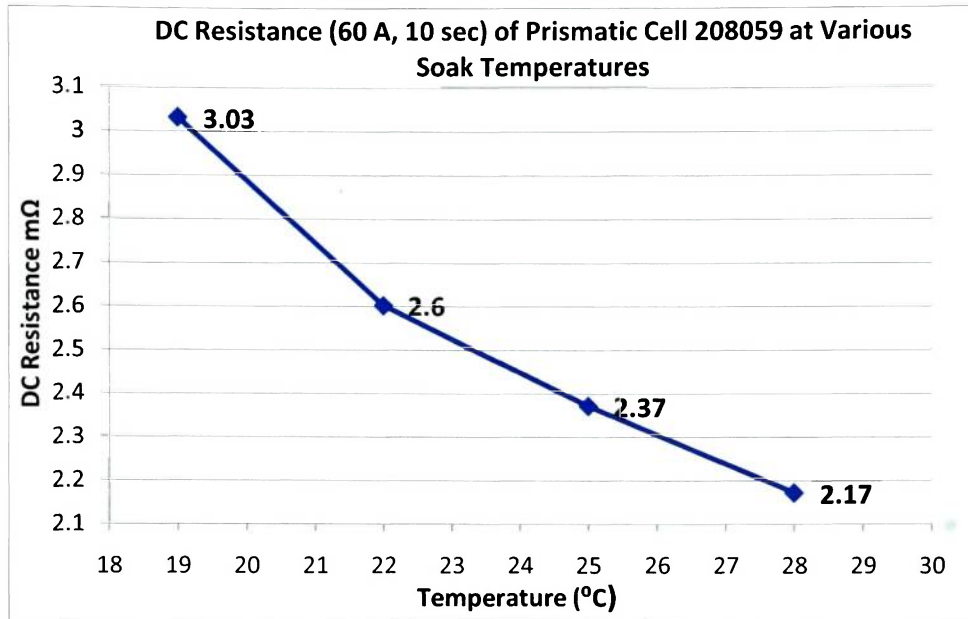


Figure 4: DC Resistance Temperature Dependence (19)

Below, Figure 5 shows an A123® prismatic module that consists of 25 pairs of 20Ah cells wired in series. The result is a module with a nominal voltage of 82.5 V and 3200 Wh of energy.

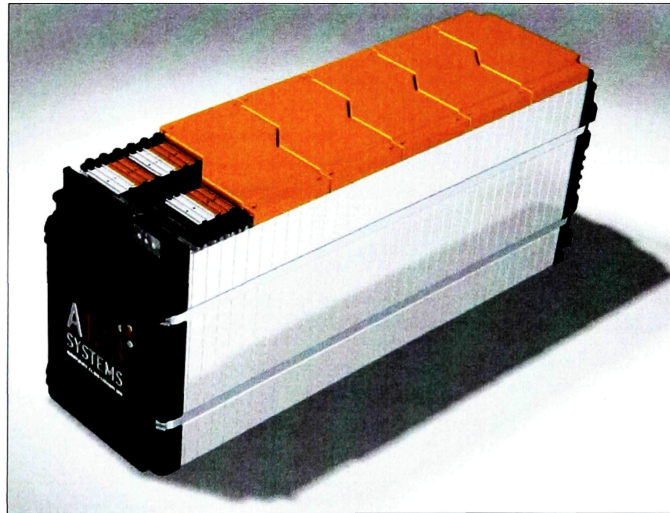


Figure 5: A123® 25S2P Prismatic Module (19)

Table 3 lists the collective properties of the A123® 20Ah cells in the form of a 25S2P module.

Table 3: 25S2P Module Properties (19)

Weight	30.4 kg
Internal Resistance (DC)	30 mΩ (@ 25 °C)
Internal Resistance (AC)	16 mΩ (@ 25 °C)
Heat Capacity	25,400 J/K

Illustrated in Figure 6 is an exploded view of the A123® 25S2P module. For the purpose of simulation, the cells were modeled as a lumped thermal mass. The pressure plates, compression straps, bolts, circuit boards, and covers would only increase the complexity of the model. These items are not in the path of conduction between the cells and the cold plate, therefore they are not considered necessary for the analysis

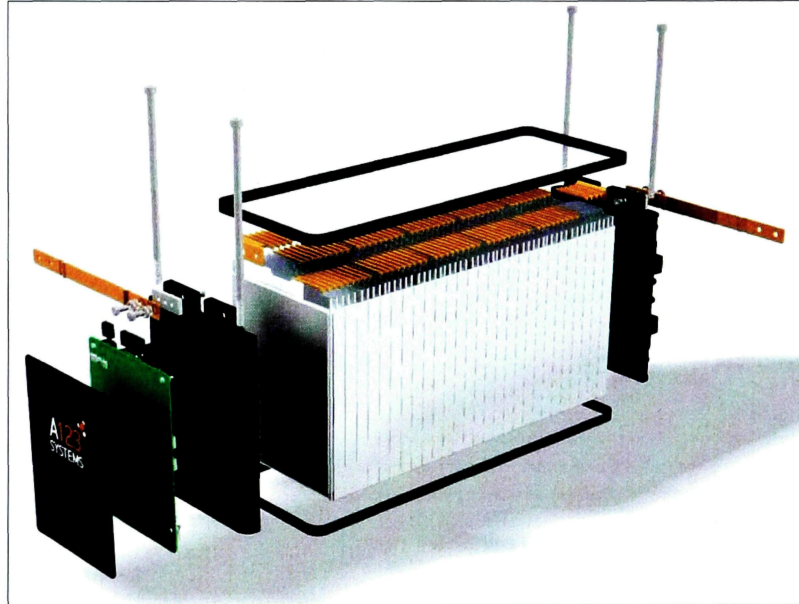


Figure 6: A123® 25S2P Prismatic Module Exploded View (19)

The simplified thermal mass (blue) model can be seen in Figure 7 with the components to be excluded from the simulation. Figure 8 shows the simplified thermal mass as it appears in the analysis.



Figure 7: SolidWorks® Model of 25S2P Module

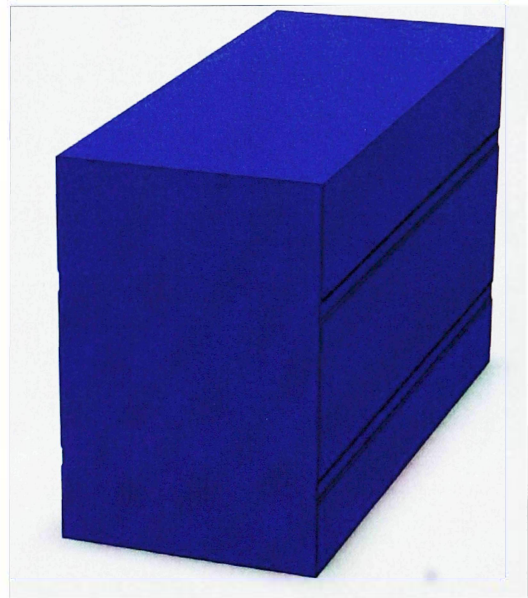


Figure 8: SolidWorks® Model of Thermal Mass

To assist with heat dissipation, foil heat sinks are interleaved between every other cell. Figure 9 and Figure 10 show the heat sink foil (in blue) attached the A123® 20Ah cells. The R-values given in Table 2 include the interleaved foil.



Figure 9: Prismatic Cell with Heat Sink Foil (19)

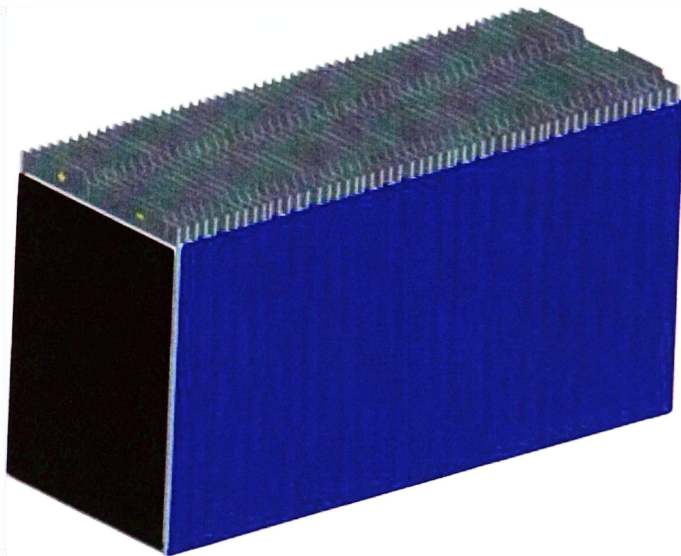


Figure 10: Prismatic Cells with Heat Sink Foil Interleaved Between Every Other Cell (19)

Energy Storage System

The ESS design for the EcoEagles vehicle integrates four of the A123® 22S2P modules in series to yield a 12.9 kWh energy storage capacity at 330V nominal. The ESS will be positioned in the rear of the vehicle, under a removable floor, where the vehicles spare tire would normally be located. The battery modules are positioned as far forward as possible to maintain a safe distance from the vehicle's rear crush zone. Figure 11 shows a model of the ESS installed in the rear of the EcoEagles Vue.

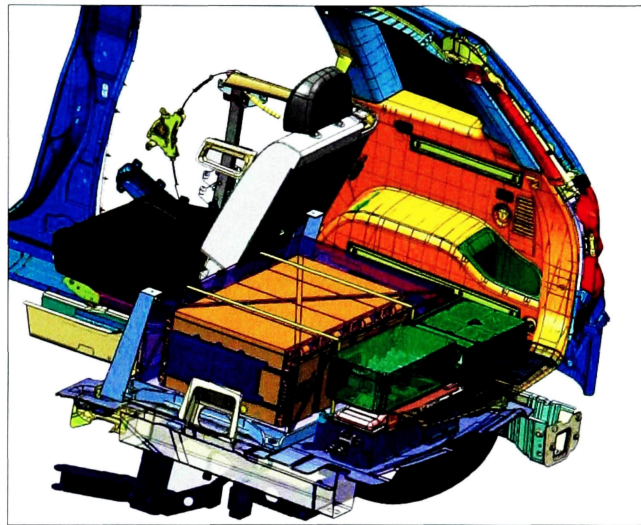


Figure 11: ESS Installed In Saturn® Vue® (21)

A side view of the ESS is illustrated in Figure 12.

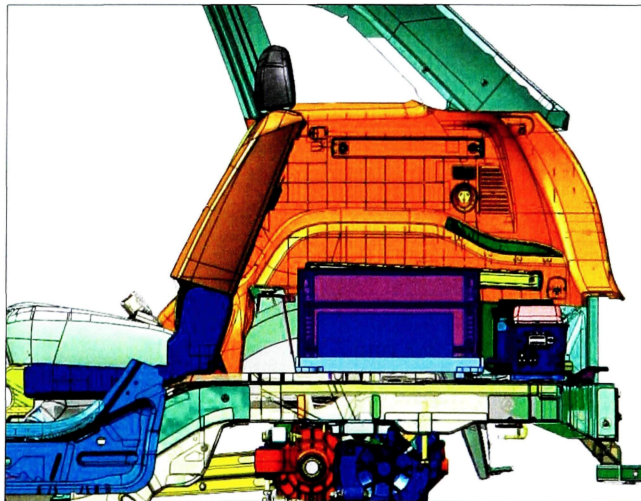


Figure 12: Side View of ESS Installed In Saturn® Vue® (22)

The liquid cooled structural cold plate that will be used to manage the temperatures of the ESS needs to be comprised of a material that is strong, lightweight, and has a high thermal conductivity. Aluminum 6061 was chosen because it satisfies the aforementioned conditions plus it is a widely available and economical alloy of aluminum. The relevant thermal properties of Aluminum 6061 can be found below in Table 4.

Table 4: Thermal Properties of Aluminum 6061 (23)(24)

Density (kg/m^3)	2700
Specific Heat Capacity ($J/kg-K$)	900
Thermal Conductivity ($W/m-K$)	180

Electrical Modeling and Simulation

In order to estimate the heat production of the modules in the ESS, simulations were performed using Argonne National Laboratory's Powertrain Simulation Analysis Toolkit (PSAT) (25). The simulated vehicle architecture is based on a Saturn® Vue® chassis with a 1.3L diesel engine, coupled to a two-mode transmission to drive the front wheels, while a 55kW electric motor drives the rear wheels. All of the electrical components including all the electric motors, are powered by an energy storage system model based on the A123® 25S2P battery pack design with four modules in series for a nominal ESS voltage of 330 V (26).

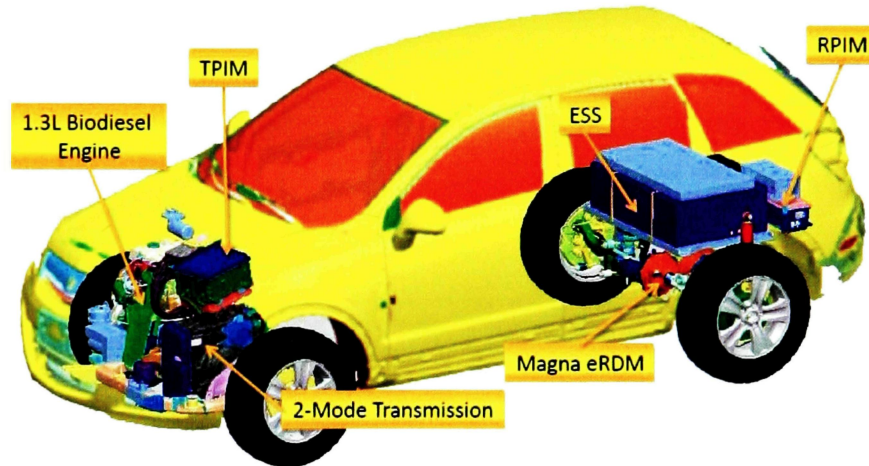


Figure 13: EcoEagles Powertrain Configuration (14)

Simulations were performed for three different drive cycles, including: city (UDDS Figure 14), highway (HWFET Figure 15), and a towing cycle that simulates towing 680 kg at a constant speed of 72 km/h for 20 minutes up a 3.5% grade. These simulations do not optimize energy use from the ESS and, consequently, represent worst-case conditions. Specifically, while the eventual control algorithms will distribute load unequally among the electric motors for higher efficiency, the PSAT models distribute loads equally (26).

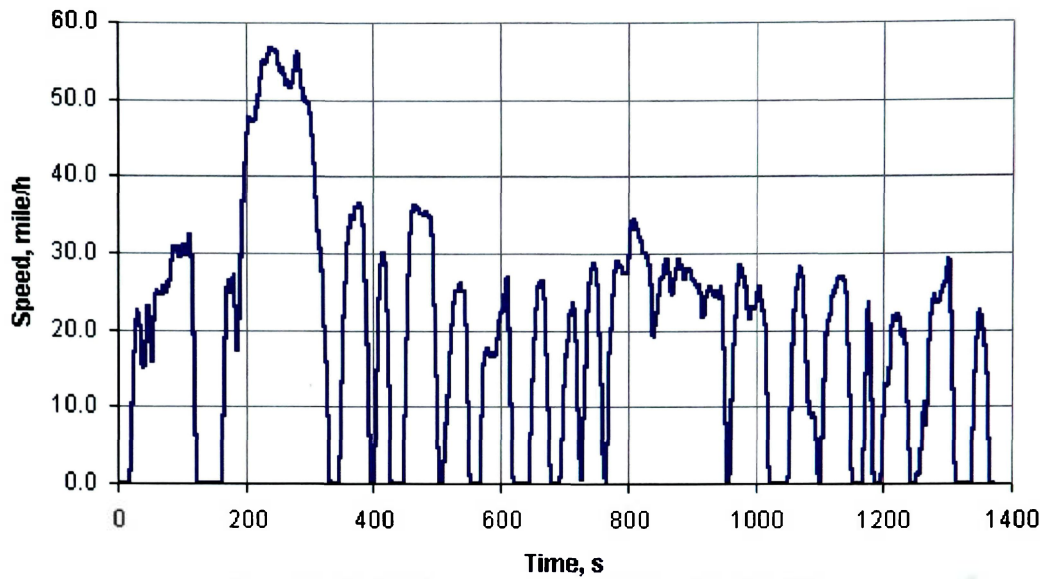


Figure 14: FTP-72 Urban Dynamometer Driving Schedule (27)

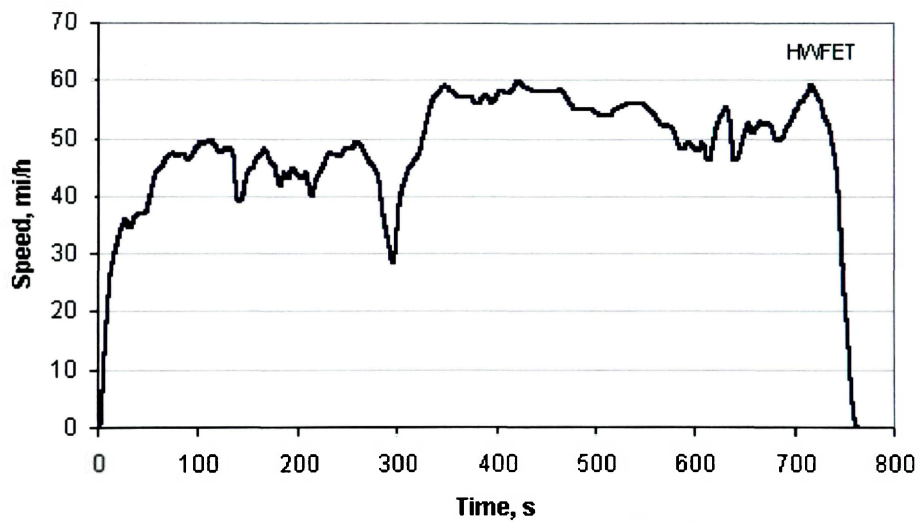


Figure 15: EPA Highway Fuel Economy Cycle (28)

The PSAT simulation data were output at 0.1 second intervals then analyzed using MATLAB® and Excel. The data consisted of current in amperes, and ESS potential in volts. The data was smoothed using boxcar averaging to obtain 0.5 second, 10 second, and 60 second data smoothing intervals. The RMS values were calculated for the smoothed data set and the maximum charge and discharge currents were found (26).

Table 5: PSAT ESS - Load Simulation Data (26)

Time Intervals		0.5 Seconds	10 Seconds	60 Seconds
City (UDDS) Current (A)	RMS	41.5	33.0	20.8
	Max (discharge)	278	159	102
	Min (charge)	-105	-102	-90.0
Highway (HWFET) Current (A)	RMS	38.9	32.2	24.0
	Max (discharge)	358	118	78.9
	Min (charge)	-112	-81.0	-31.9
Towing Current (A)	RMS	65.6	65.8	66.7
	Max (discharge)	190	178	143
	Min (charge)	-2.53	-0.015	-0.03

The 60 sec towing current is the highest RMS current value. Therefore, the thermal management system will be evaluated on its ability to dissipate the heat produced from a continuous 66.7A discharge.

Heat Production in Battery Modules

Heat is generated in a battery cell by entropy change from electrochemical reactions and Joule's effect (ohmic heating) caused by current transfer across internal resistances and over-potential. In some cases, heat generation occurs from overcharging a fully charged cell. The heat generation rate of a cell is calculated as follows (29):

$$\dot{Q} = -I \left(T \frac{dE}{dT} \right) + I(E - V)$$

Where:

\dot{Q} = Heat generation rate (W)

I = Current (A)

T = Temperature (K)

dE/dT = Temperature coefficient (V/K)

E = Equilibrium cell voltage or open-circuit potential (V)

V = Cell voltage or cell potential (V)

At practical HEV charge/discharge rates, the first term is small compared to the second (ohmic heating) (29). Therefore, for this analysis only the ohmic heating is considered. The heat produced by each A123® battery pack is calculated using the 60 sec towing current from Table 5.

$$\dot{Q} = I^2 R = (66.7 \text{ A})^2 (27.1 \text{ m}\Omega) = 121 \text{ W}$$

The resistance used is the DC resistance of a 25S2P battery module at 28 °C because this is the highest temperature value available (Figure 4). At the time of the analysis, the estimation of the 60 sec towing heat generation rate was 123 W. Since it is the goal of the cooling system to prevent the battery packs from overheating, the 2 W difference will only increase the margin of safety in the design and was not considered to be a significant enough change to re-run the analysis.

Software: SolidWorks® 2009 Flow Simulation

SolidWorks® Flow Simulation was selected as the analysis software because of its simulation capabilities in addition to its 3-D CAD platform. The following physical capabilities of Flow Simulation make it possible to perform the thermal analysis of the ESS (30):

- External and internal fluid flows
- Steady-state and time-dependent fluid flows
- Compressible gas and incompressible fluid flows
- Subsonic, transonic, and supersonic gas flows
- Free, forced, and mixed convection
- Fluid flows with boundary layers, including wall roughness effects
- Laminar and turbulent fluid flows
- Heat conduction in fluid, solid with/without conjugate heat transfer and/or contact heat resistance between solids and/or radiation heat transfer between opaque solids, and/or volume (or surface) heat sources
- Various types of thermal conductivity in solid medium
- Real gases
- Relative humidity in gases and mixtures of gases

Flow Simulation is capable of predicting both laminar and turbulent flows (31). Laminar flows occur at low values of the Reynolds number, which is defined as the product of representative scales of velocity and length divided by the kinematic viscosity. When the Reynolds number exceeds a certain critical value, the flow becomes turbulent, i.e. the flow parameters start to fluctuate randomly (30).

Flow Simulation, like other CFD software, solves the Navier-Stokes equations (32), which are formulations of mass, momentum and energy conservation laws for fluid flows (30). The equations are supplemented by fluid state equations defining the nature of the fluid, and by

enabling the user to use temperature dependent properties when available (33). Figure 16 and Figure 17 show the values for the specific heat of water and aluminum used in the analysis. Other material properties used in the thermal analysis, such as thermal conductivity, and density, do not vary adequately over the temperature range to warrant temperature dependent values. The thermal properties of the battery modules were specified by A123® as constant values. Therefore, temperature dependent values for its properties were not considered.

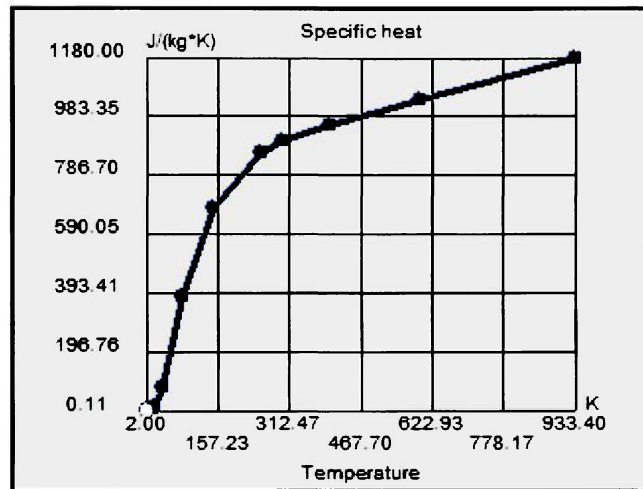


Figure 16: Specific Heat of Aluminum (34)

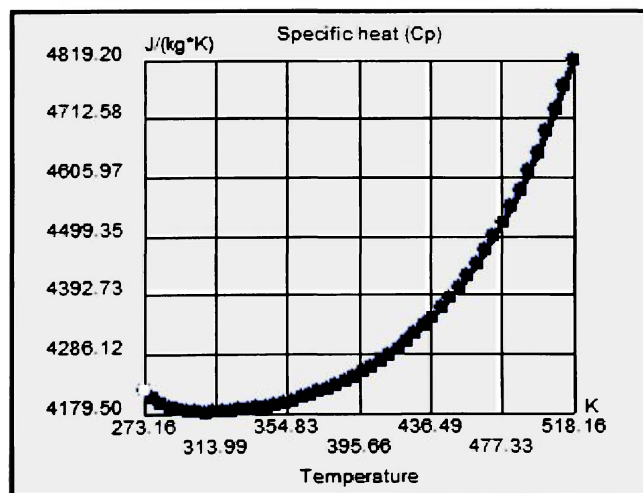


Figure 17: Specific Heat of Water (35)

Flow Simulation allows one to predict simultaneous heat transfer in solids and fluids with energy exchange between them, also known as conjugate heat transfer. Heat transfer in fluids is described by the energy conservation equation (30):

$$\frac{\partial \rho H}{\partial t} + \frac{\partial \rho u_i H}{\partial x_i} = \frac{\partial}{\partial x_i} (u_i (\tau_{ij} + \tau_{ij}^R) + q_i) + \frac{\partial p}{\partial t} - \tau_{ij}^R \frac{\partial u_i}{\partial x_j} + \rho \varepsilon + S_i u_i + Q_H$$

$$H = h + \frac{u^2}{2}$$

Where:

ρ = Fluid density

S_i = Mass distributed external force per unit mass

Q_H = Heat source per unit volume

τ_{ij} = Viscous shear stress tensor

q_i = Diffusive heat flux

where the heat flux is defined by:

$$q_i = \left(\frac{\mu}{Pr} + \frac{\mu_t}{\sigma_c} \right) \frac{\partial h}{\partial x_i}, i = 1, 2, 3.$$

Here the constant $\sigma_c = 0.9$, Pr is the Prandtl number, and h is the thermal enthalpy. The phenomenon of anisotropic heat conductivity in solid media is described by the following equation (30):

$$\frac{\partial \rho e}{\partial t} = \frac{\partial}{\partial x_i} \left(\lambda_i \frac{\partial T}{\partial x_i} \right) + Q_H$$

where e is the specific internal energy, $e = cT$, c is specific heat, Q_H is specific heat release (or absorption) per unit volume, and λ_i are the eigenvalues of the thermal conductivity tensor. It is supposed that the thermal conductivity tensor is diagonal in the considered coordinate system.

For an isotropic medium $\lambda_1 = \lambda_2 = \lambda_3 = \lambda$ (30).

If a solid consists of several different materials attached to each other, then the thermal contact resistances between them (on their contact surfaces), specified in the SolidWorks® engineering database in the form of contact conductance (as $m^2 \cdot K/W$), can be taken into account when calculating the heat conduction in solids. As a result, a solid temperature step appears on the contact surfaces. In the same manner, i.e. as a thermal contact resistance, a very thin layer of another material between solids or on a solid in contact with fluid can be taken into account when calculating the heat conduction in solids, but it is specified by the material of this layer and thickness (30).

Assumptions

The following assumptions were made for the thermal analysis of the ESS. The average high temperature in Yuma, Arizona in June is approximately 40 °C (36). It is assumed that the vehicle will not be stored in an air conditioned garage prior to testing. As a result, the ambient temperature and initial ESS temperature is assumed to be 40 °C (313.15 K). Also, the rate of heat transfer from the battery modules to the coolant is assumed to occur much faster than the rate of convection from the battery modules to the cabin air. While the goal is to minimize the operating temperature of the ESS, the system should support a heat transfer rate of at least 492W when the ESS temperature reaches 50 °C (323.15 K).

Analysis Assumptions:

1. 492 W of heat distributed equally throughout the modules of the ESS (towing drive cycle).
2. Each module is modeled as a homogeneous mass (thermal characteristics and heat production).
3. Constant DC internal resistance of modules (no temperature dependence).
4. Ambient air temperature is 40 °C with 0% humidity at 1 *atm*.
5. The ESS is soaked to the ambient temperature at initialization.
6. Heat is only transferred out of the system at the heat exchanger by convection.

By assuming no heat is lost through radiation or through contact with ambient air ensures that the analysis provides a conservative estimate of the cooling system's performance.

CHAPTER 3: ANALYSIS

This chapter covers the evaluation of the thermal management system's performance. A description of the design is also presented in this section. The implications of the results are addressed as they relate to design of ESS components.

Cold Plate Design and Analysis

The ESS cooling system is designed to allow the vehicle to operate normally up to an ambient temperature of 40 °C. From the towing drive cycle, the EcoEagles vehicle yields a P_{RMS} of 123 W per pack. Therefore, the cooling system must dissipate 492 W total at temperatures as high as 40 °C (313.15 K) without allowing the packs to reach 50 °C (313.15 K) at the hottest point.

The cooling plate design includes an aluminum structural cooling plate with integrated coolant channels to support forced liquid cooling. The plate is fabricated with machined waterways which are then covered with an aluminum contact plate attached at the peripheral joints. Coolant is distributed in parallel to four U-shaped channels to minimize thermal differential between modules and from end to end along the modules. Other, more intricate, channel geometries were not used because of the difficulty associated with creating a satisfactory seal with the aluminum top plate.

Figure 18 shows a simplified model of the battery module and cold plate assembly. Features on the periphery of the cold plate that negligibly affect the heat transfer to the coolant were removed from the model to reduce the memory requirements of the simulation. Such features are the mounting locations and stiffening ribs. Also, the four cooling channel are normally separated from the batteries by a 2.5 mm aluminum plate. In this simplified model, the cold plate is modeled as a single plate rather than two plates with a thermal contact surface.

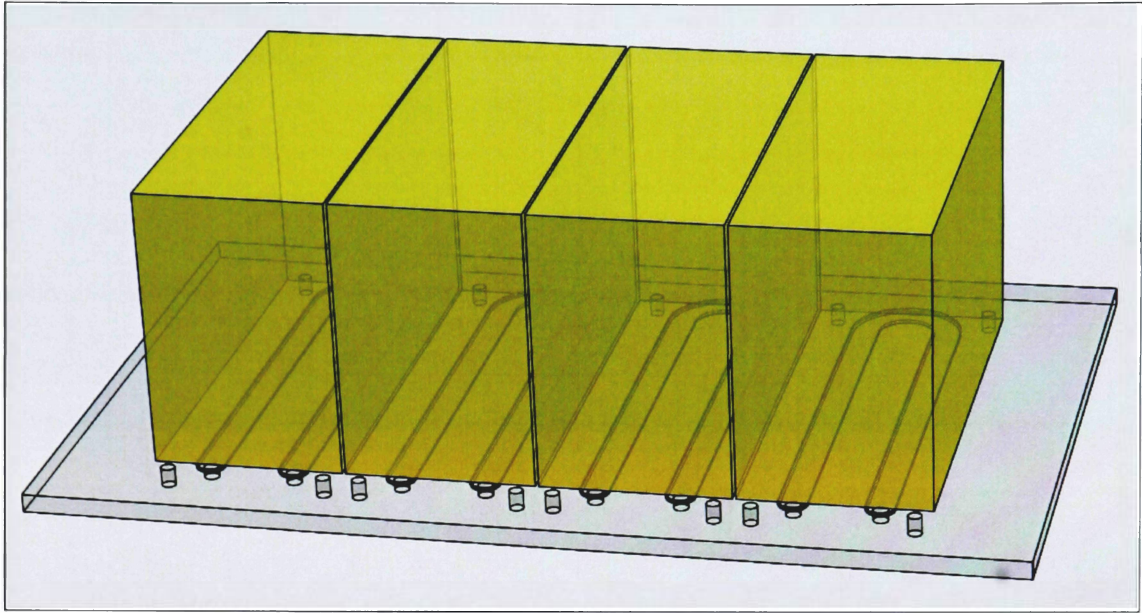


Figure 18: Simplified CAD Model of Cold Plate and Battery Modules

Basic properties of the cooling system can be found below in Table 6. Distilled water was selected for the coolant in extreme heat conditions because of its high specific heat compared to mixtures of glycol and water (37). Since thermal failure of the batteries is unlikely to occur at temperatures below the freezing point of water, an antifreeze mixture can be added to the coolant when freezing is a concern.

Table 6: Cooling System Properties

Coolant Specific Heat (<i>Distilled Water</i>)	4.19 kJ/kg K
Desired Coolant Flow Rate	0.4 kg/s
P_{RMS}	492 W
Δ Coolant Temperature	0.29 K

The coolant flow rate was selected based on the availability of flow rates for automotive coolant pumps as well as the desire to minimize the ΔT of the coolant. In order to absorb the heat from the ESS at the desired flow rate, the coolant temperature must increase by the amount calculated below:

$$\Delta T_{Coolant} = \frac{492 J/s}{\left(0.40 \text{ kg/s}\right) \left(4.19 \text{ kJ/kg K}\right)} = 0.29 \text{ K}$$

A confirmation of the 0.29 K temperature rise in the coolant as it passes through the cold plate can be seen in Figure 19. More specifically, Figure 19 shows flow traces of the coolant in the cold plate where the colors correspond to temperature.

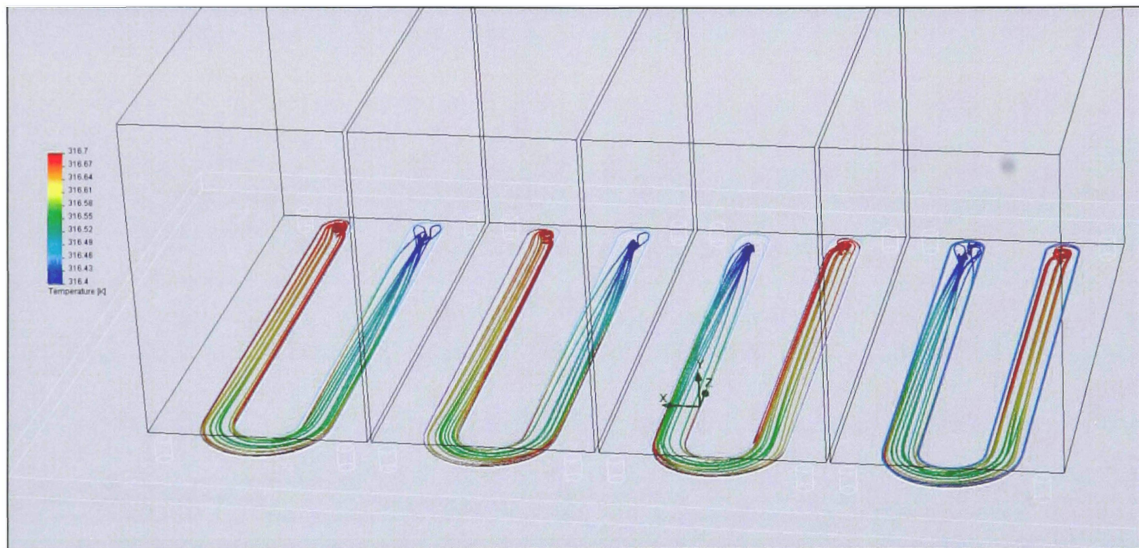


Figure 19: Flow Trace of Coolant through Cold Plate Showing Coolant Temperature

Due to the thermal conductivity of the battery packs the maximum allowable average surface temperature of the cold plate is 44.5 °C (317.6 K) to ensure the battery packs are just below 50 °C (323.15 K) in desert conditions. The following two illustrations (Figure 20 and Figure 21) show the temperature distribution of the cold plate's top surface. The difference between the hottest and coldest point is only 0.7 K.

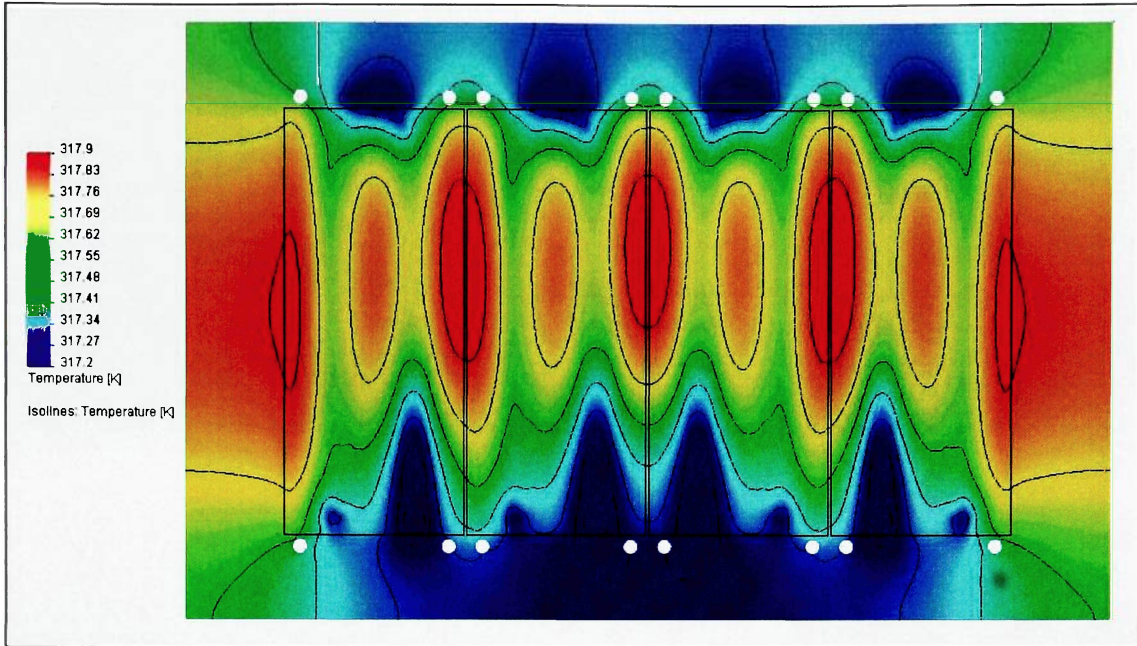


Figure 20: Surface Temperature of Cold Plate (Top View)

The black rectangles in Figure 20 represent the locations of the battery modules on the surface of the cold plate. Figure 21 illustrates the coolant temperature relative to the surface of the cold plate.

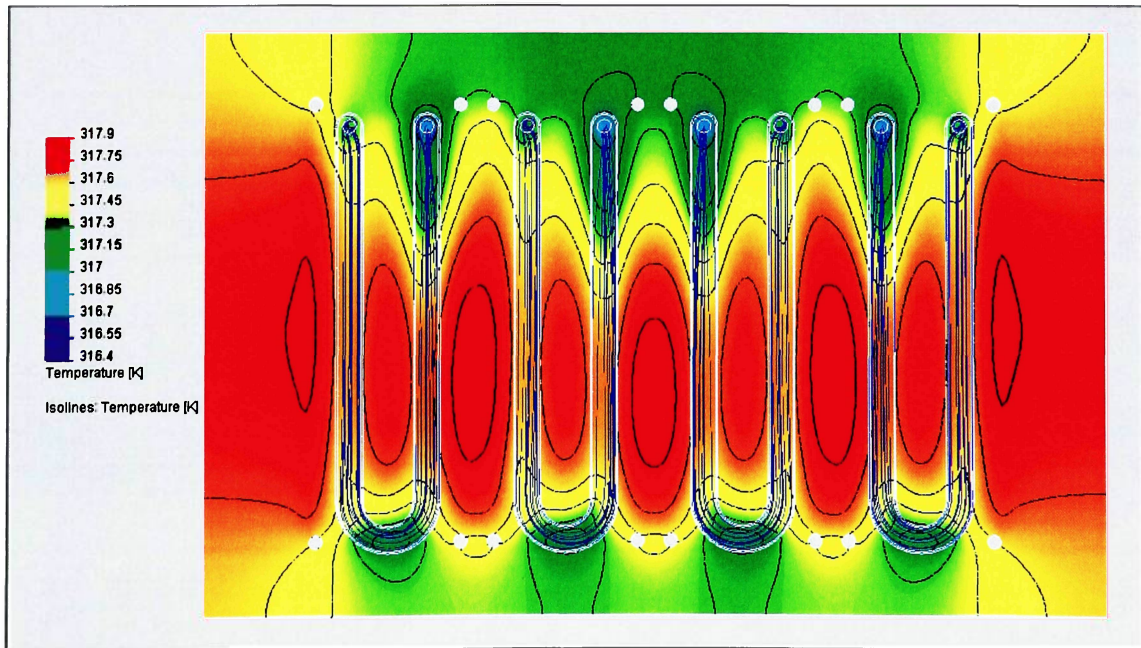


Figure 21: Surface Temperature of Cold Plate with Coolant Flow Traces (Bottom View)

Figure 22 depicts the temperature distribution in the center of the battery packs as seen from the front of the ESS. The top of the modules just reach 50 °C (323.15 K) at a P_{RMS} of 492 W.

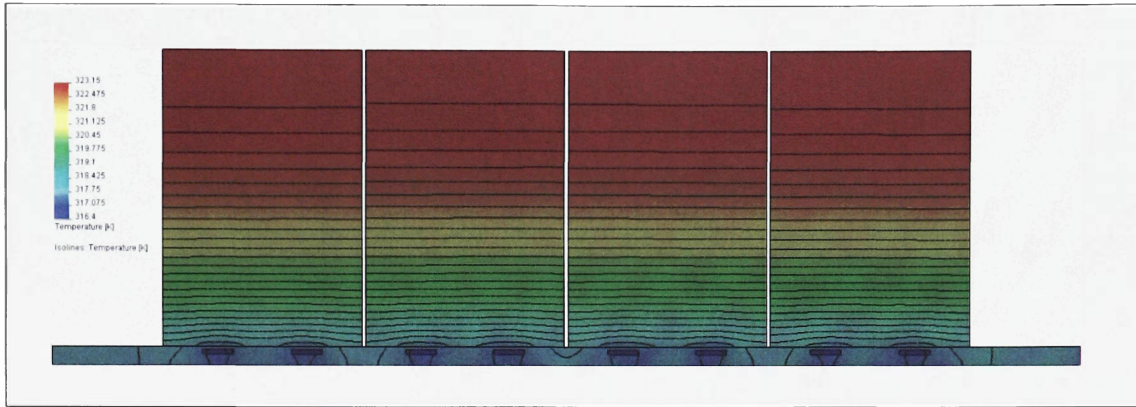


Figure 22: Center Temperature of ESS (Front View)

As can be seen in Figure 22 and Figure 23 the variations in the surface temperature of the cold plate have minimal effect on the uniformity of the temperature at the top of the battery modules.

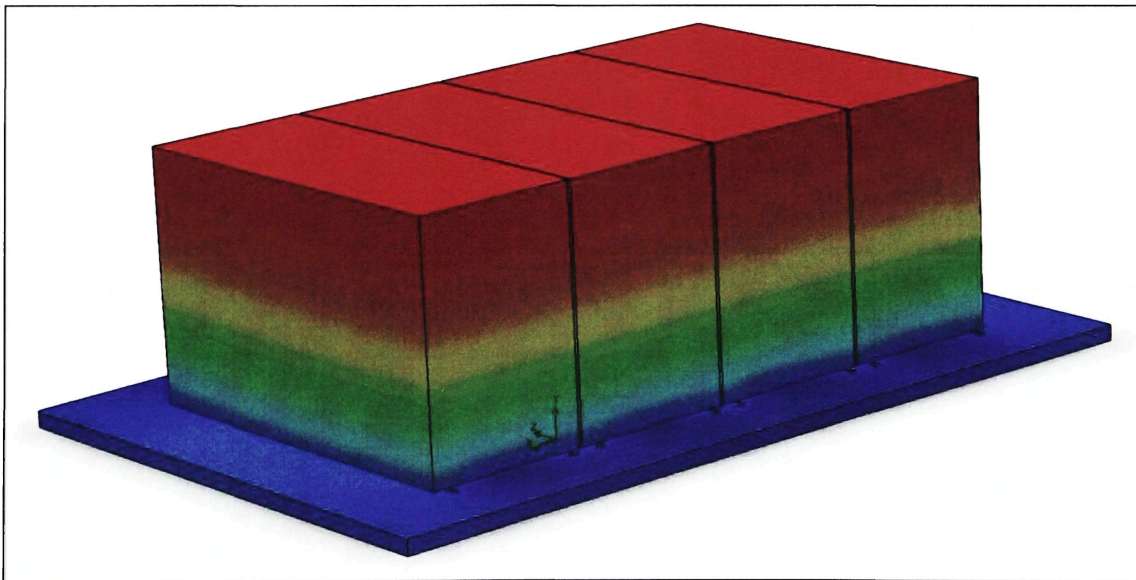


Figure 23: Surface Temperature of ESS

Figure 24 illustrates the changes in pressure (ΔP) of the coolant throughout the cold plate. The change in pressure is used later to determine the total ΔP for the system.

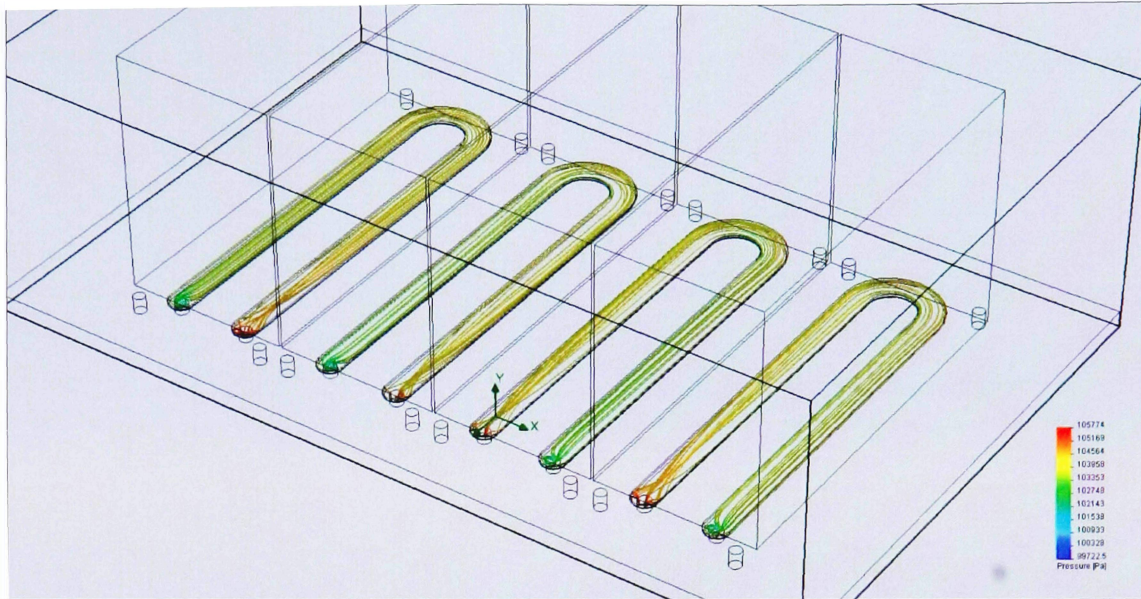


Figure 24: Flow Trace Through Cold Plate Showing Coolant Pressure

Cold Plate Analysis Summary

The analysis of the ESS was performed using SolidWorks® Flow Simulation. The model was simplified into five parts: four battery modules and the aluminum cold plate. The boundary conditions and heat sources are listed below and shown in Figure 25.

Boundary Conditions and Heat Sources:

1. Inlet mass flow of 0.4 kg/s at 43.15 °C (316.4 K) distributed to the four channels
2. Outlet at environmental pressure (101,325 Pa)
3. Real wall condition on upper surface of cooling channels (50 micrometer roughness)
4. 492 W of heat produced evenly among the four modules
5. Adiabatic wall conditions on outer surfaces of the ESS

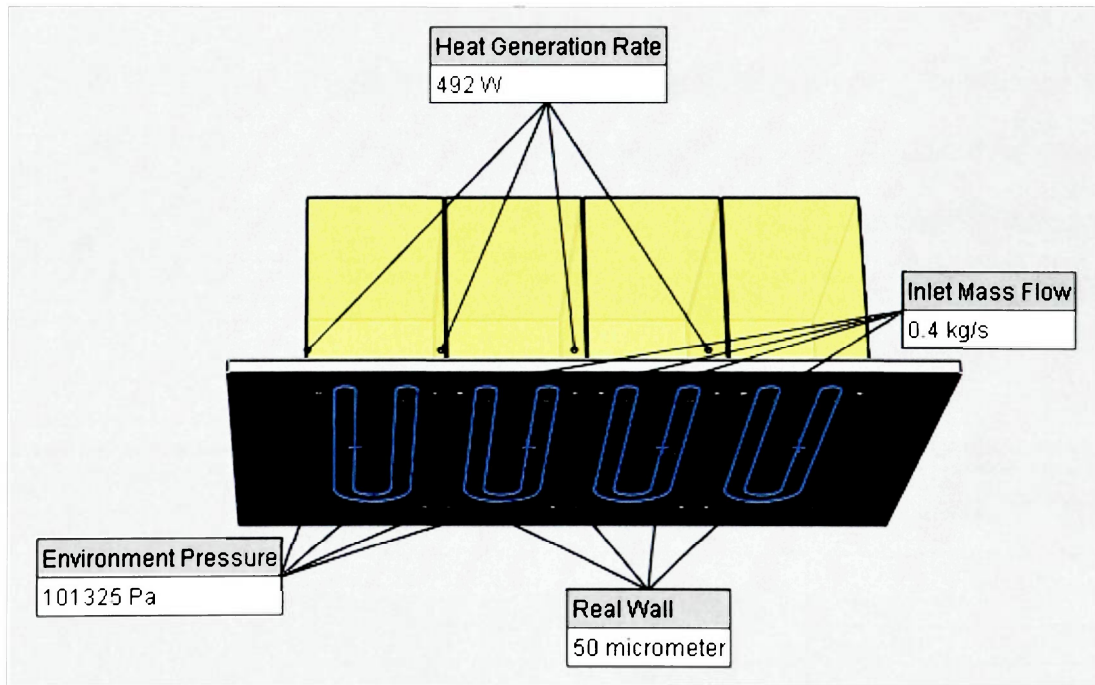


Figure 25: Cold Plate Boundary Conditions and Heat Sources

Since the simulation's goal is to find the steady-state solution, the initial conditions are not vital to the accuracy of the simulation. Even so, the values were still considered and all materials in the model started at 40 °C.

The intricacy of the model can be estimated from the solver parameters in Table 7. To give the CPU time more relevance, the analysis was performed on a 64-bit platform with an Intel® Core™ 2 Duo P8600 CPU at 2.40 GHz with 6 GB of RAM (38).

Table 7: Cold Plate Solver Parameters

Fluid Cells	139,553
Solid Cells	1,356,308
Partial Cells	307,509
Iterations	275
CPU Time (sec)	12,231

For steady-state problems solved by an iterative approach it is necessary to properly select the termination moment for the calculation. Termination of the calculation before initial condition induced transients have damped down sufficiently can result in errors in the results while using an excessive number of iterations can waste computational resources. To optimize the termination point for the calculation and to determine more accurately the physical parameters of interest which oscillate in iterations (average temperature of a surface or static pressure) the user may specify physical parameters of interest as the calculation goals (39). The selected parameters of interest can be found in Table 8.

Table 8: Cold Plate Solver Goal Parameters

Goal Name	Value	Delta	Achieved at Iteration #
Average Exit Temperature of Coolant	316.704 K	0.0011217	244
Bulk Average Exit Temperature of Coolant	316.695 K	0.0011241	244
Heat Flux Through Cold Plate Surface	1070.24 W/m ²	0.0048107	244
Static Pressure of Coolant at Entrance	105,205 Pa	76.1714	275
Average Temperature of A123® Module Tops	323.116 K	0.0029756	244
Average Surface Temperature of Cold Plate	317.575 K	0.0033657	244

Fluid Path Design and Analysis

The acceptable temperature range of the ESS is much lower than all of the other liquid cooled systems on the EcoEagles Vue. Consequently, the ESS coolant loop must be isolated from all other cooling systems on the vehicle. Figure 26 shows the coolant paths on the EcoEagles vehicle. One option for the placement of the ESS heat exchanger would be to position it in front of the Internal Combustion Engine (ICE) heat exchanger and the Transmission Power Inverter Module (TPIM) heat exchanger. However, not enough information was known about the air flow rates over the TPIM and ICE heat exchangers to validate the design. Space limitations as well as high ambient heat in the front of the vehicle also make such a design decision unattractive.

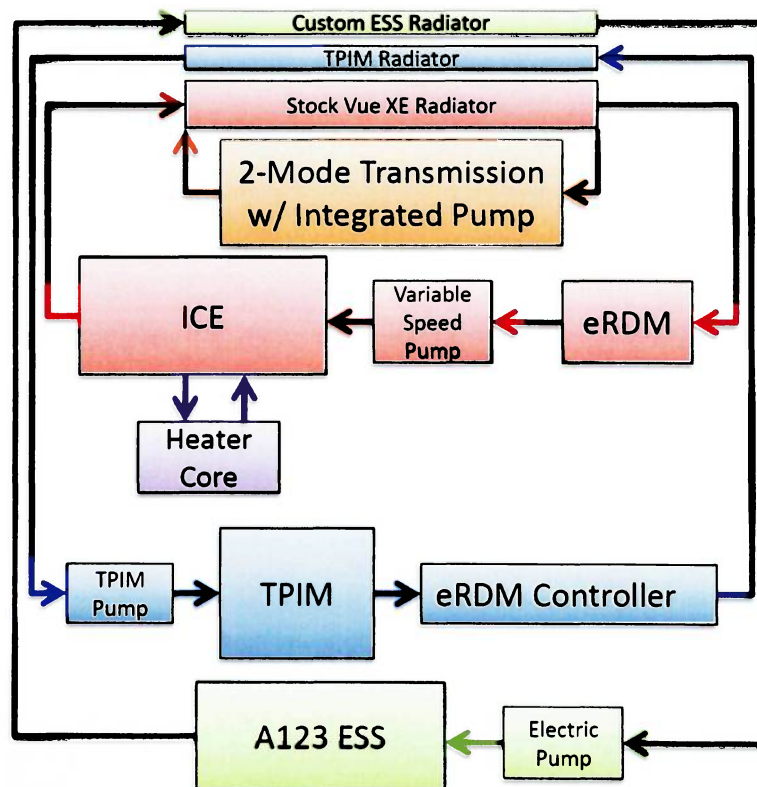


Figure 26: Coolant Paths (40)

Instead, a design that could operate independently of the other heat exchangers is more desirable. More specifically, a design that can adequately cool the ESS at all vehicle speeds is one which the required airflow rate is low enough so that fans can supply it. The heat exchanger must also be able to transfer the 492W produced by the ESS to the ambient air at a very low temperature differential. Figure 27 shows the selected heat exchanger for the ESS thermal management system.

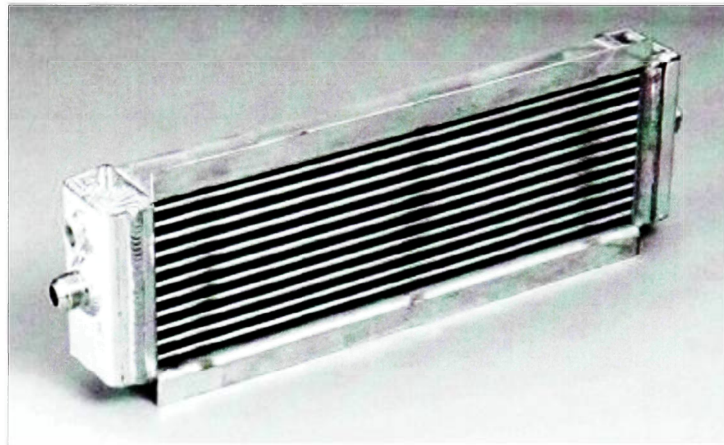


Figure 27: Fluidyne® DB-30618 Heat Exchanger (533 x 150 x 76 mm) (41)

Due to large memory requirements associated with meshing intricate structures, a simplified version of the heat exchanger was modeled to reduce the computational burden. It is assumed that if the simplified heat exchanger satisfies the design requirements that the actual heat exchanger (with a larger surface area to volume ratio) will exceed the performance of the simplified model. The simplified model consists of a single aluminum tube with 100 vertical fins attached to it.

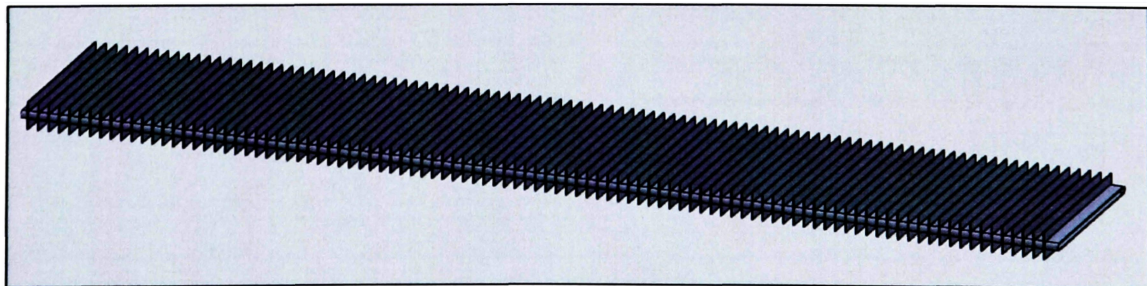


Figure 28: Fluidyne® Heat Exchanger Simplified CAD Model

More detailed properties of the heat exchanger model can be found in Table 9.

Table 9: Fluidyne® Heat Exchanger Model Properties

Material	Aluminum 6061
Tube Outside Dimension	3.2 x 76.2 x 445 mm
Wall Thickness	0.5 mm
Tube Spacing	9.9 mm
Fin Thickness	0.4 mm
Number of Fins	100

To ensure sufficient airflow is present across the heat exchanger regardless of vehicle speed, electric fans were selected to force the airflow. SPAL produces a fan that fits the height of the heat exchanger core. Three of these fans will be used across the width of the heat exchanger.

Figure 29 illustrates the major dimensions of the SPAL VA67-A101-83A fans selected.

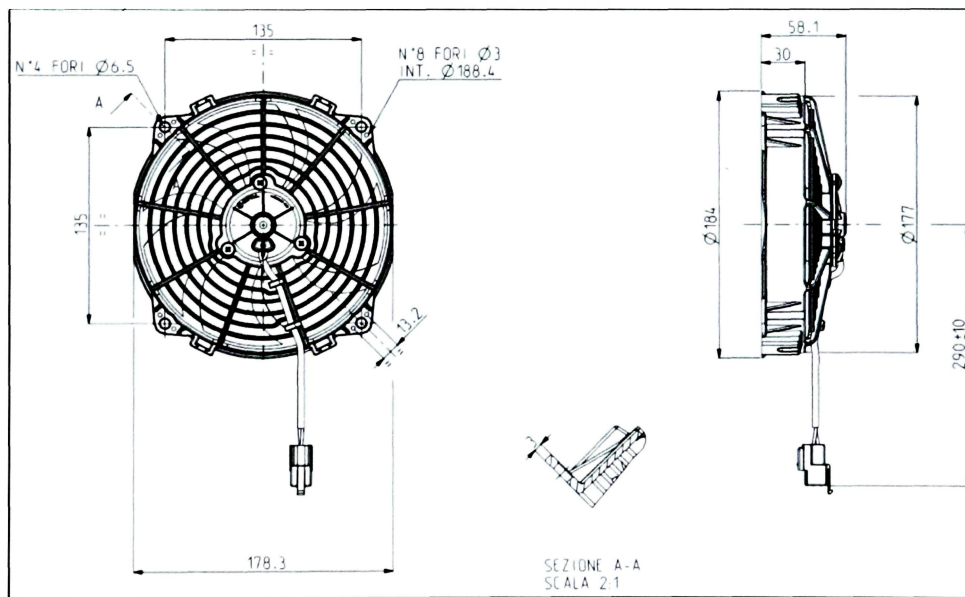


Figure 29: SPAL VA67-A101-83A Fan (42)

To determine the flow rate across the heat exchanger, it is necessary to determine the pressure loss as air flows over the exchanger. Table 10 compares the fan's flow rate to the static pressure.

Table 10: SPAL Fan Airflow at 13V (42)

Static Pressure (Pa)	Airflow (m ³ /h)	Current Input (A)
0	550	3.9
49	500	4.2
74	470	4.4
98	440	4.4
123	410	4.6
147	380	4.6
17.5	350	4.9
172	300	4.9
245	190	5.6
294	100	5.8
343	0	6.2

The SPAL fans are rated at 500 m³/h at 49 Pa. As can be seen in Figure 30, the pressure change across the heat exchanger is no more than 20 Pa.

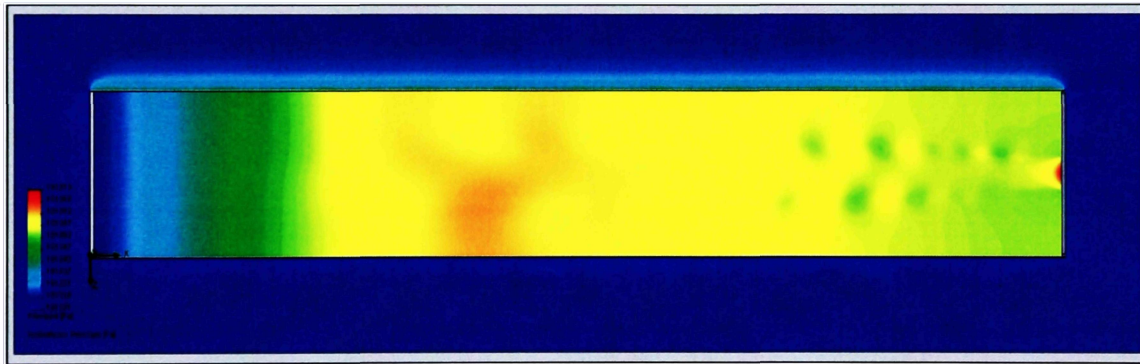


Figure 30: Fluid Pressure along Heat Exchanger Core Centerline

For the analysis, 6 m/s of air flow across the heat exchanger was selected to dissipate the heat from the ESS because this value is less than 1500 m³/h. The following calculation verifies that three SPAL fans provide the desired air flow over the heat exchanger.

$$\text{Volumetric Flow Rate}_{\text{air}} = (0.064 \text{ m}^2)(6 \text{ m/s})(3600 \text{ s/hr}) = 1392 \text{ m}^3/\text{hr}$$

The corresponding mass flow rate is as follows.

$$\text{Mass Flow Rate}_{\text{air}} = (0.064 \text{ m}^2)(6 \text{ m/s}) \left(1.185 \frac{\text{kg}}{\text{m}^3} \right) = 0.46 \text{ kg/s}$$

With 0.46 kg/s of air flowing over the heat exchanger, the required temperature rise to dissipate 492 W is calculated as follows.

$$\Delta T_{air} = \frac{492 \text{ J/s}}{\left(0.46 \text{ kg/s}\right) \left(1.01 \text{ kJ/kg K}\right)} = 1.06 \text{ K}$$

The results shown in Figure 31 confirms the 1.06 K temperature rise as the air passes over the heat exchanger.

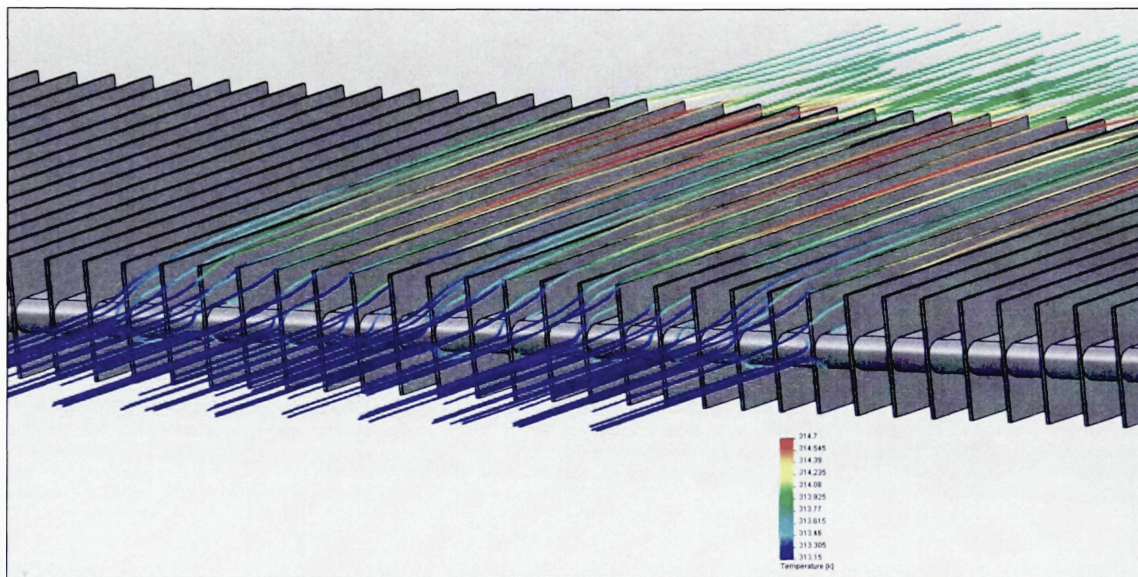


Figure 31: Flow Trace over Heat Exchanger Core Showing Air Temperature

The temperature distribution on the surface of the heat exchanger is shown in Figure 32. The colder blue region is the downstream side of the heat exchanger whereas the yellow region is the upstream side.

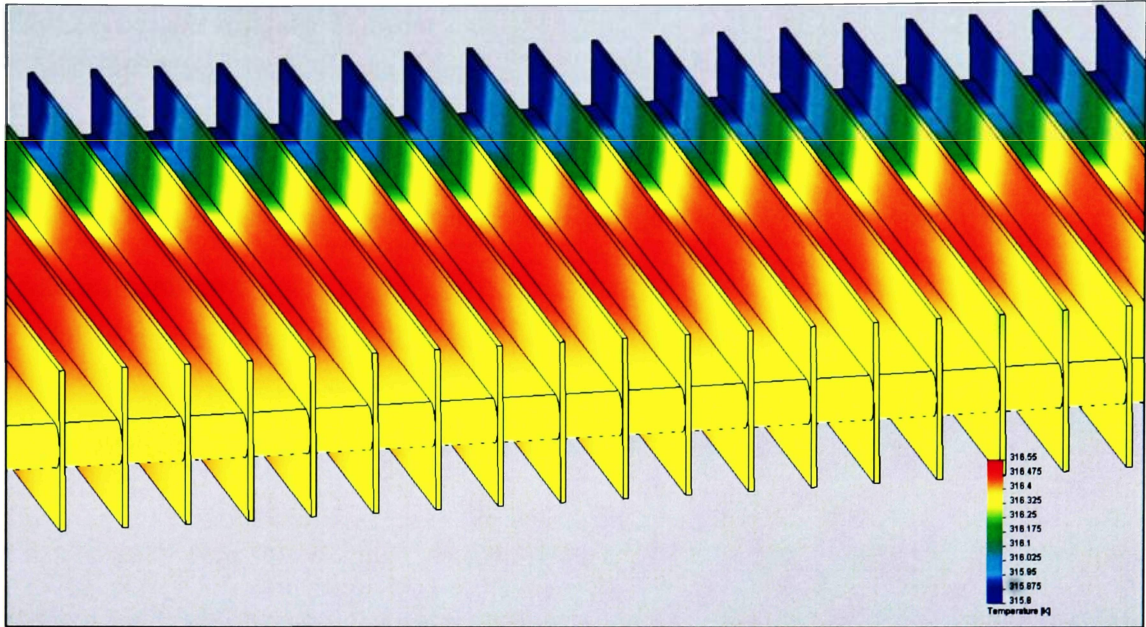


Figure 32: Surface Temperature of Heat Exchanger Core

A section view along the centerline of the heat exchanger tube as seen from the top illustrates the temperature of both the air and coolant (Figure 33). The coolant flows from right to left in the illustration and the top of the illustration is the upstream side of the heat exchanger.

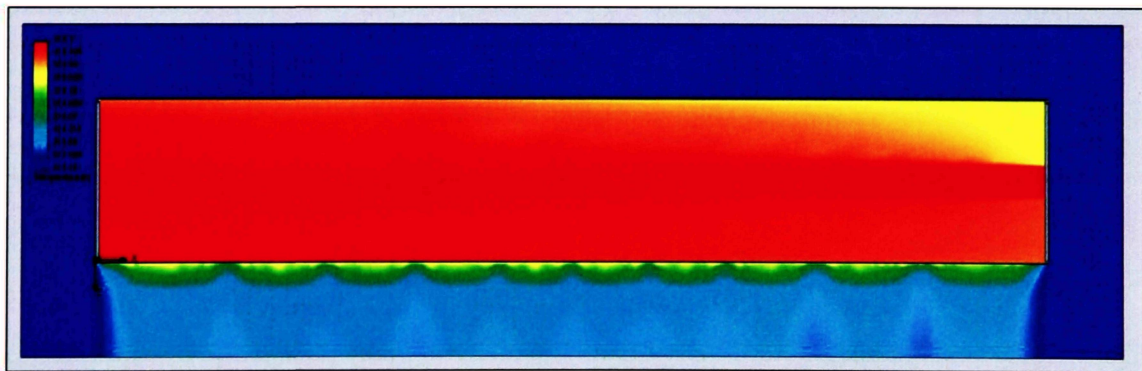


Figure 33: Fluid Temperature along Heat Exchanger Core Centerline

Heat Exchanger Analysis Summary

SolidWorks® Flow Simulation was used for the analysis of the heat exchanger similarly to the analysis of the cold plate. Unlike the cold plate model, the heat exchanger model was able to be simplified into a single part. The boundary conditions of the model are shown below.

Boundary Conditions:

1. Inlet mass flow rate of 0.033 kg/s at 42.5 °C (316.65 K)
2. Outlet at environmental pressure (101,325 Pa)
3. Ambient airflow of 6 m/s at 101,325 Pa and 40 °C (313.15 K)

The inlet mass flow rate is 1/12th of the system's total flow rate because the modeled heat exchanger is 1/12th (one row) of the actual heat exchanger. Also, all materials in the model had an initial temperature of 40 °C (313.15 K). Details of the analysis can be found in Table 11.

Table 11: Heat Exchanger Solver Parameters

Fluid Cells	327,893
Solid Cells	428
Partial Cells	227,035
Iterations	318
CPU Time (sec)	30,299

The goals of the heat exchanger analysis are shown in Table 12. The outlet temperature and inlet pressure were the primary parameters of interest.

Table 12: Heat Exchanger Solver Goal Parameters

Goal Name	Value	Delta	Achieved at Iteration #
Average Exit Temperature of Coolant	316.408 K	0.0041289	318
Average Entrance Static Pressure of Coolant	101,356 Pa	2.40878	165

Coolant Pressure Calculations

The determination of the pressure losses in the coolant path is necessary to ensure a given pump can produce the desired coolant flow rate. The following equations were used to determine the pressure drop across the cooling system (43).

$$Re = \frac{\text{Internal forces}}{\text{Viscous forces}} = \frac{V_{avg} D}{\nu} = \frac{\rho V_{avg} D}{\mu}$$

For flow through non circular pipes, the Reynolds number is based on the hydraulic diameter D_h defined as

Hydraulic diameter:
$$D_h = \frac{4A_c}{p}$$

Where A_c is the cross-sectional area of the pipe and p is its wetted perimeter. The hydraulic diameter is defined such that it reduces to ordinary diameter D for circular pipes,

Circular pipes:
$$D_h = \frac{4A_c}{p} = \frac{4(\pi D^2/4)}{\pi D} = D$$

For rectangular ducts,

Rectangular duct:
$$D_h = \frac{4A_c}{p} = \frac{2ab}{a + b}$$

Where a and b are the height and width of the duct respectively.

Pressure Loss:
$$\Delta P_L = f \frac{L}{D} \frac{\rho V_{avg}^2}{2}$$

Where $\rho V_{avg}^2 / 2$ is the dynamic pressure and f is the Darcy friction factor,

Darcy friction factor:
$$f = \frac{8\tau_w}{\rho V_{avg}^2} = \frac{64}{Re}$$

The pressure and flow properties of the cooling system can be found in Table 13.

Table 13: Coolant Path Properties

Cold Plate Channel Cross-section	1 in x 0.15 in (0.0254 m x 0.0038 m)
Cold Plate Channel Length	32 in (0.81 m)
Channel Average Velocity	1.08 m/s
Channel Hydraulic Diameter	0.0066 m
Channel Re	10866
Channel ΔP	421 Pa (0.061 psi)
Connective Tubing Diameter	0.75 in (0.019 m)
Connective Tubing Length	25 ft (7.62 m)
Average Velocity in Tubing	1.45 m/s
Tubing Re	42229
Tubing ΔP	645 Pa (0.094 psi)

Figure 34 indicates a 6.90 kPa (1 psi) pressure drop across the Fluidyne® DB-30618 heat exchanger. This pressure drop is using oil (higher viscosity than water) and a flow rate of 0.88 l/s (14 GPM) which is greater than twice the flow rate required. Therefore, it is assumed that the change in pressure across the heat exchanger is less than 6.90 kPa.

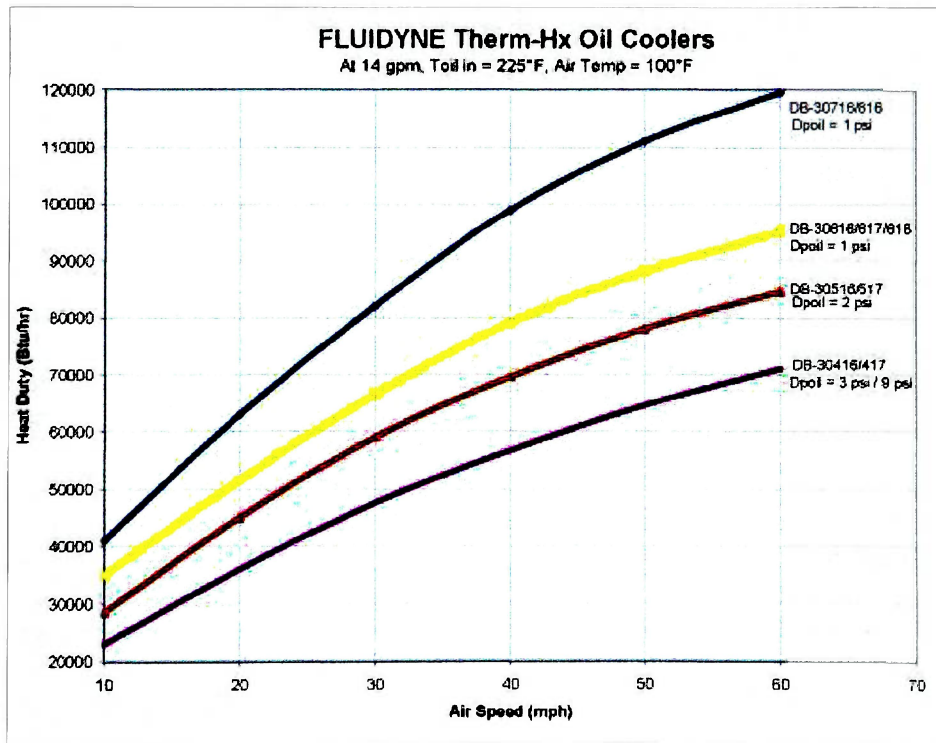


Figure 34: Fluidyne® Heat Exchanger Performance (44)

In order to give the design flexibility in terms of rerouting tubing and changing flow rates, a Dedenbear pump was selected that can provide the required flow rate at pressure much higher than actually seen by the system (Figure 35).



Figure 35: Dedenbear WP3 Water Pump (45)

The performance specifications of the Dedenbear WP3 water pump can be seen below in Table 14.

Table 14: Dedenbear WP3 Water Pump Specifications (45)

Voltage	12 V
Current	3 A
Flow Rate	0.4 kg/s @ 51.7 kPa
Inlet/Outlet Diameter	0.75 in

The pressure drop across the heat exchanger is at most 6.90 kPa when flowing motor oil at 0.88 l/s so it is assumed that the pressure drop is less than 6.90 kPa, but for pump sizing purposes, 6.9 kPa will be used in the estimates. Therefore the total pressure drop in the cooling system is 6.90 kPa + 0.65 kPa + 0.44 kPa = 7.99 kPa. The pump selected is capable of producing a flow rate of 0.4 kg/s at pressures as high as 51.7 kPa.

Sensitivity Analysis

Of the parameters affecting the performance of the thermal management system, the flow rates of the coolant and air have the greatest impact on the design (46). As can be seen in Figure 36, the water flow rate was intentionally selected so that it was greater than the point of diminishing return with respect to change in temperature for a given power. The flow rate of 0.4 kg/s (6.3 GPM) was selected in order to reduce the temperature variations in the cold plate surface by minimizing the temperature changes in the coolant. This flow rate is also justified by the availability of automotive grade coolant pumps that exceed the desired flow rate.

Table 15: Fluid Flow Rates vs. ΔT

Parameter	Diminishing Return Above
Air Flow Rate	1000 m ³ /s
Water Flow Rate	0.13 l/s
50% EGW	0.14 l/s

The air flow rate over the heat exchanger was selected to allow the system to operate close to the thermal limit of the batteries. This also caused the air flow rate to be higher than point of diminishing return. The air flow rate required in extreme temperatures, approximately 1400 m³/s (820 CFM), is much greater than that required for a few degrees cooler. Figure 38 illustrates the effectiveness of a flow rate at a given heat production rate. Even though the flow rate is higher than the most effective rate, it is not difficult to produce with fans.

It is due to the packaging requirements and operating temperature range of the ESS that the system's flow rates must be greater than optimal for the system to function. If the battery modules were cooled from the sides (lower R-value than from the bottom) or the temperature margin was increased, then the flow rates could be reduced so that the heat transfer occurs at a more efficient temperature differential.

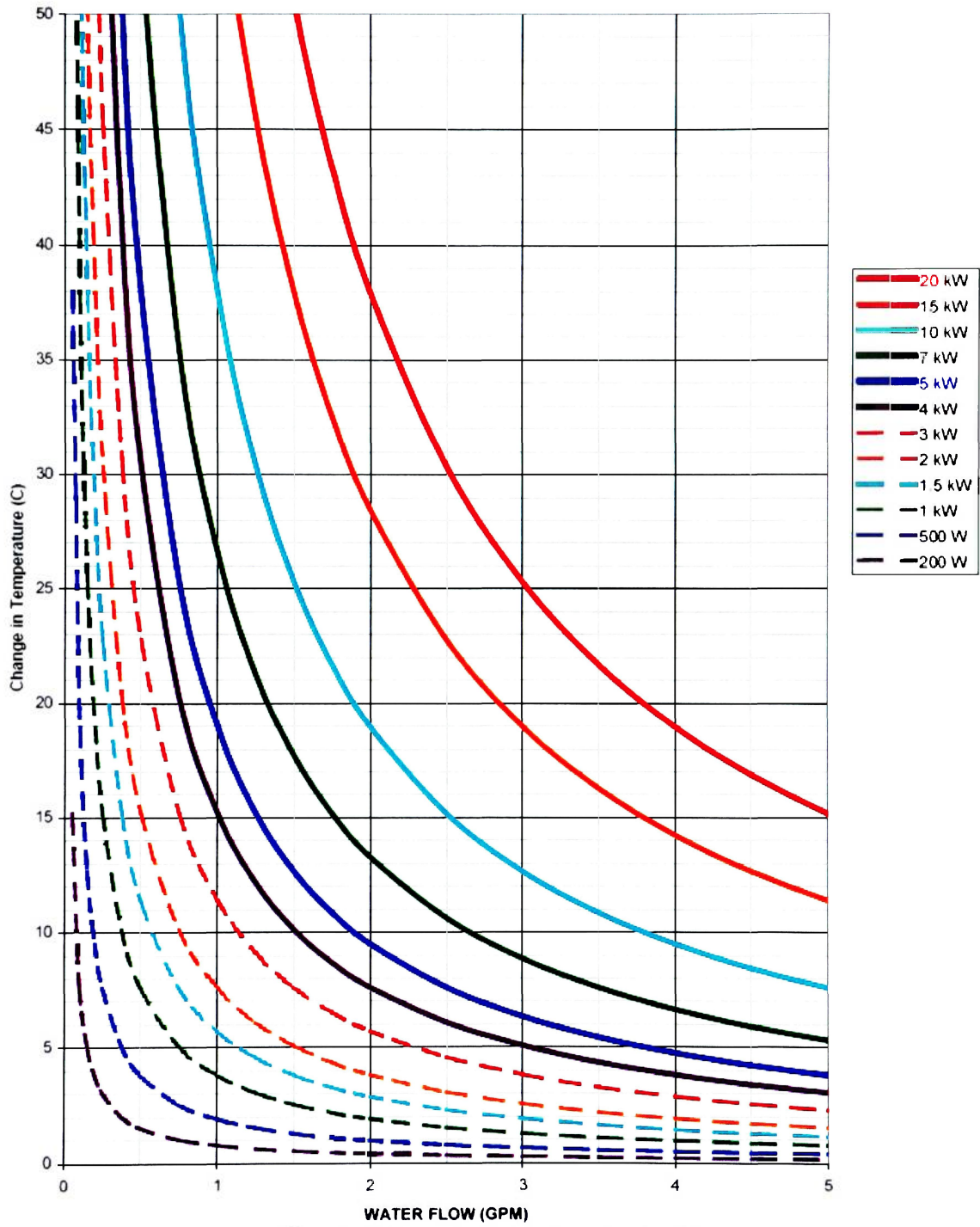


Figure 36: Water Temperature Change Chart (47)

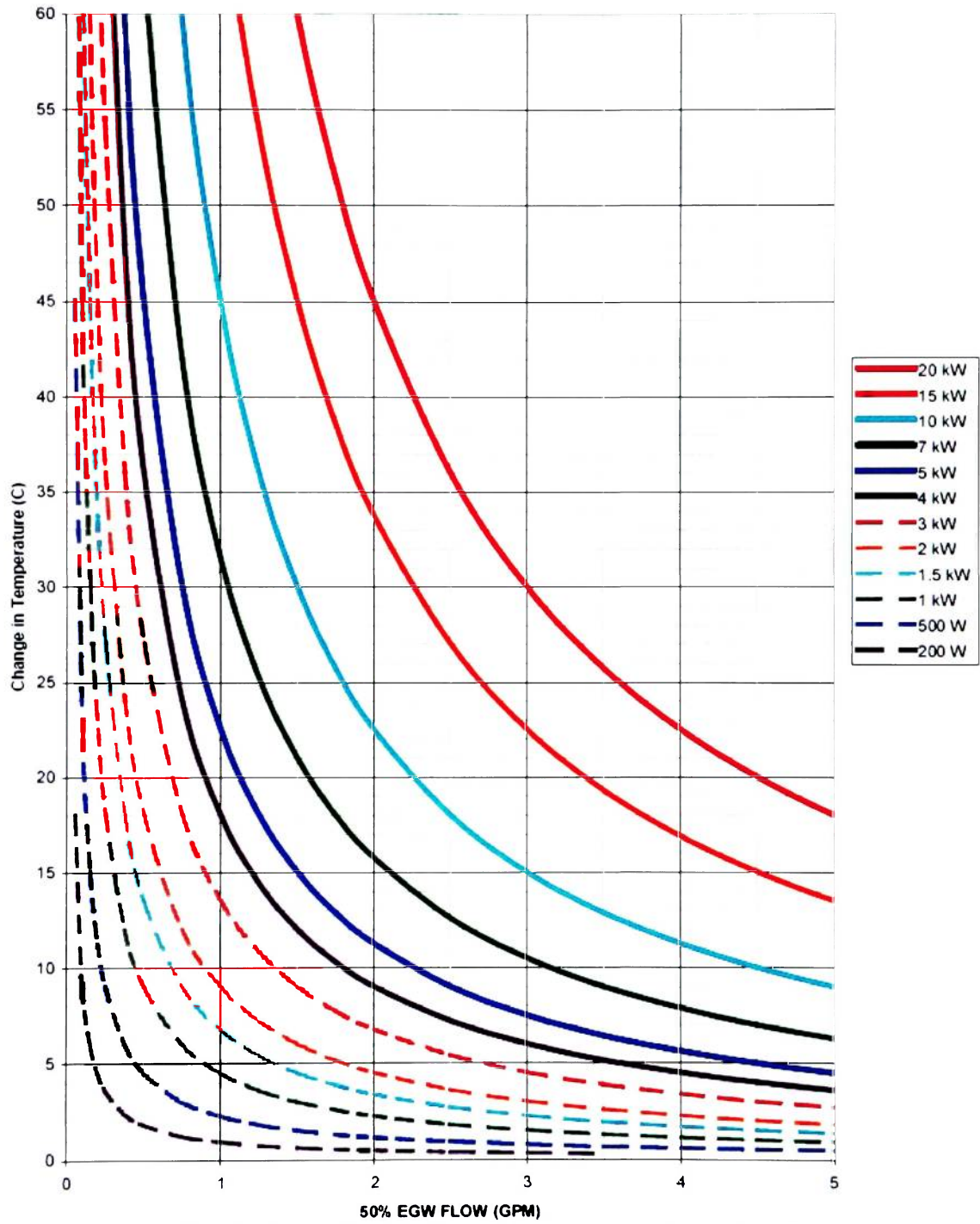


Figure 37: 50% Ethylene Glycol and Water Temperature Change Chart (47)

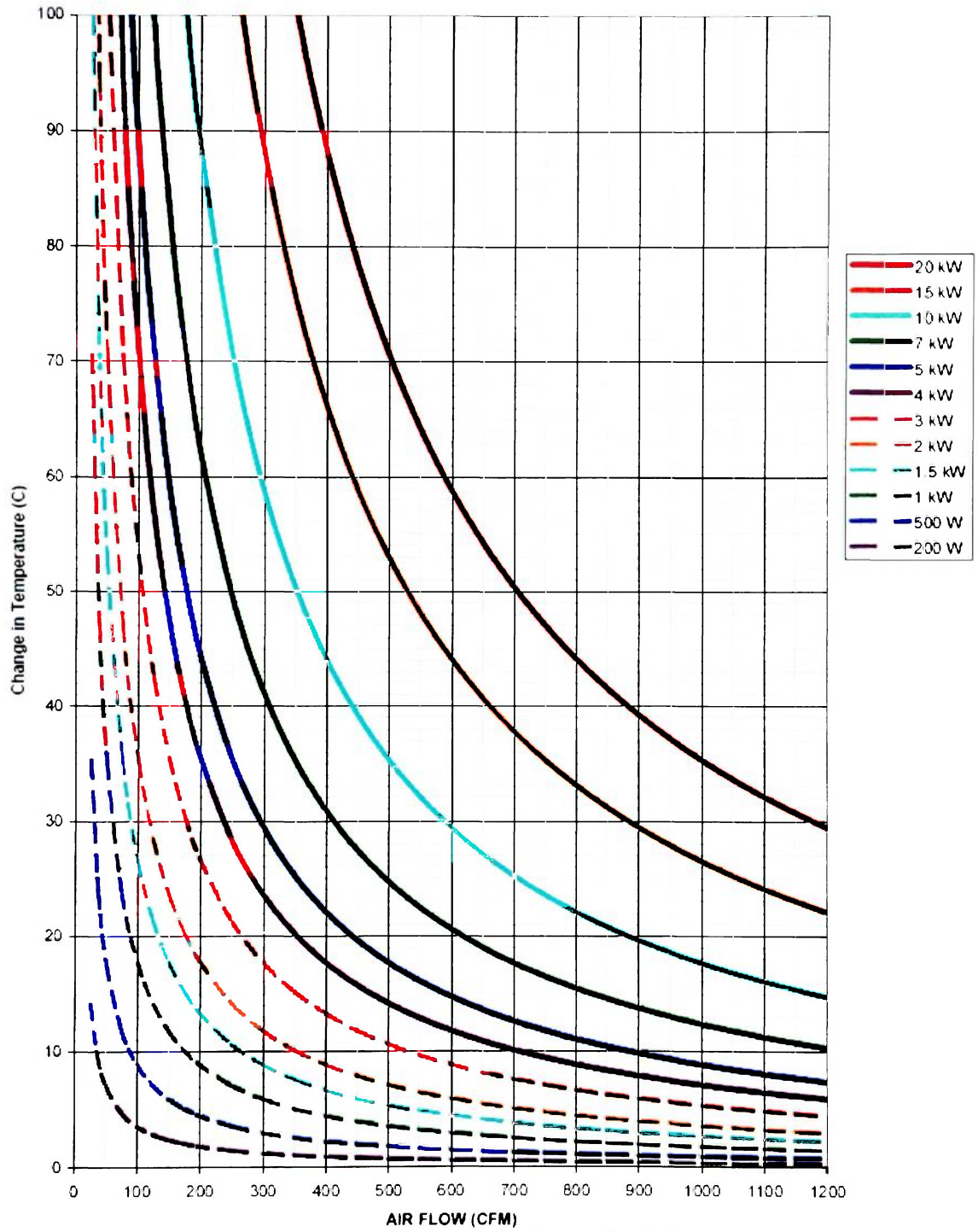


Figure 38: Air Temperature Change Chart (47)

CHAPTER 4: CONCLUSION

This chapter provides a summary of the research presented in the previous chapters. It also provides a description of the results as well as their relation to the design of the EcoEagles Vue.

Summary of Analysis

The thermal management of batteries is a vital aspect of safe and efficient operation of HEVs. Assuming that the ESS is electrically isolated properly, thermal failure of the batteries poses the greatest risk. Reducing the hazards associated with Li-Ion batteries is crucial to their commercial implementation in HEVs. Considering the effects of temperature on batteries, one can realize the need for establishing more accurate relationships between current and battery temperature distribution.

Several design/analysis iterations were performed before an appropriately sized thermal management system was achieved. The analysis started with the modeling of the cold plate and battery modules. Once temperature distribution was verified to be uniform, the inlet coolant temperature was increased until the tops of the battery modules were slightly below 50 °C. Holding the temperature of the batteries slightly below their limit enables the heat exchanger to operate at a larger temperature differential.

The next step was to use the data from the cold plate analysis to size a heat exchanger for the system. The analysis of the heat exchanger proved to be the most difficult because it must operate at very constricted temperature margins. Many iterations were undertaken to balance performance and packagability. The initial designs were found to be undersized after analysis. The difficulty in sizing the heat exchanger can be attributed to the lack of information available

from the manufacturers. However, the data gained from the analysis of the undersized heat exchangers was useful in the selection of the current heat exchanger.

Finally, the pressure losses seen in the cold plate and heat exchanger were used to select a coolant pump. The greatest challenge with the analysis was the latency in determining whether a simulation would produce a good result once it had been initialized. This can cause serious time delays when some of the failed analyses ran for over 32 hours. Fortunately, the delays did not cause the analysis to fall behind schedule.

Variations in Ambient Temperature

The results of the analysis can be approximated as linear with respect to the ambient air temperature. Since radiation is assumed not to contribute significantly to the heat transfer from the system, the remaining heat transfer mechanisms (conduction and convection) are dependent on the relative temperature, not absolute. Therefore, if the ambient temperature were to drop, the peak battery temperature will drop by approximately the same amount. There are, however, temperature dependent properties, such as DC resistance of the cells, that affect the results of the analysis at different temperatures. These changes are relatively small over the operating range of the vehicle and are safe to neglect as long as this approximation is not used to validate ambient temperatures over 40 °C.

ESS Assembly

The final ESS design consists of an arrangement of four A123® 25S2P modules attached to a structural aluminum cooling plate shown in Figure 39. In the event that a battery cell overheats, the ESS is sealed and vented to the outside in order to prevent the gasses from being released in the cabin. In the assembly there are several modules that control the flow of current through the batteries. These modules can also be used to regulate the current as the temperature of the batteries rise to prevent overheating.

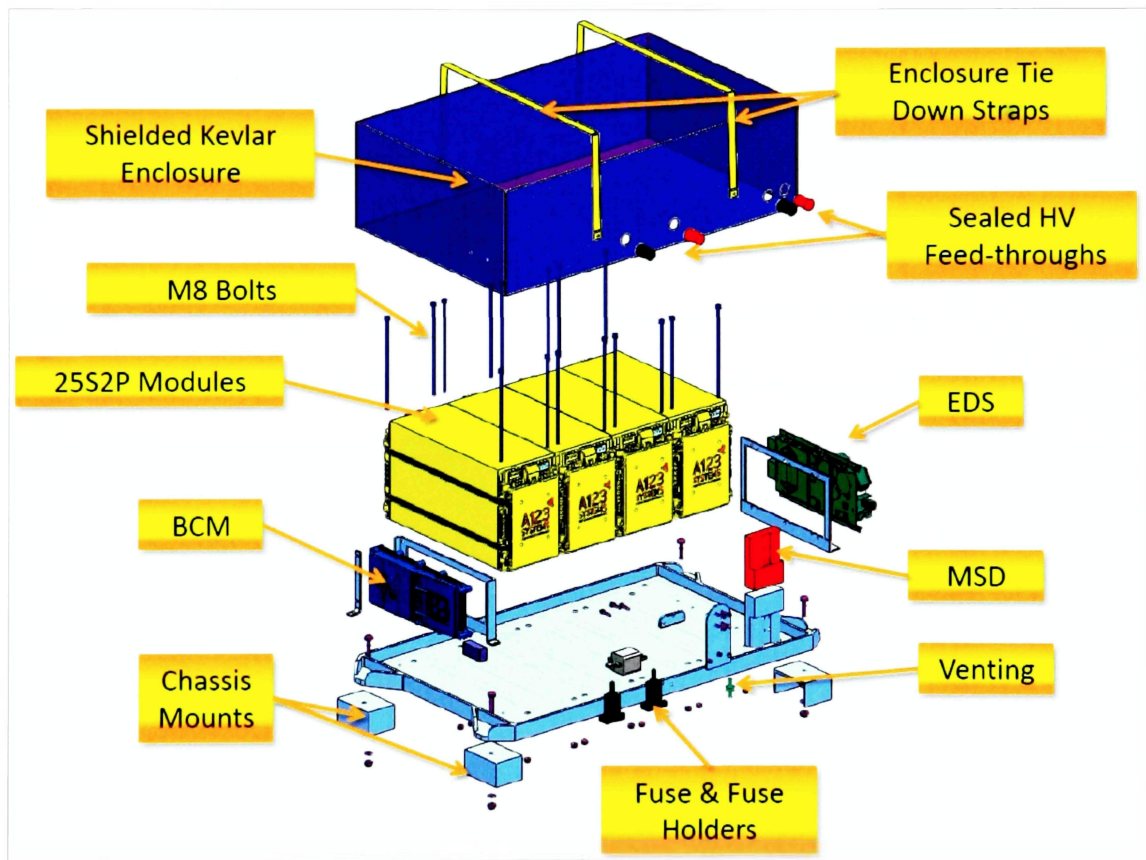


Figure 39: Exploded ESS Component Assembly (26)

The finished structural cold plate can be seen below in Figure 40 post machining. The top plate will be attached to the structural cold plate to seal the coolant path.

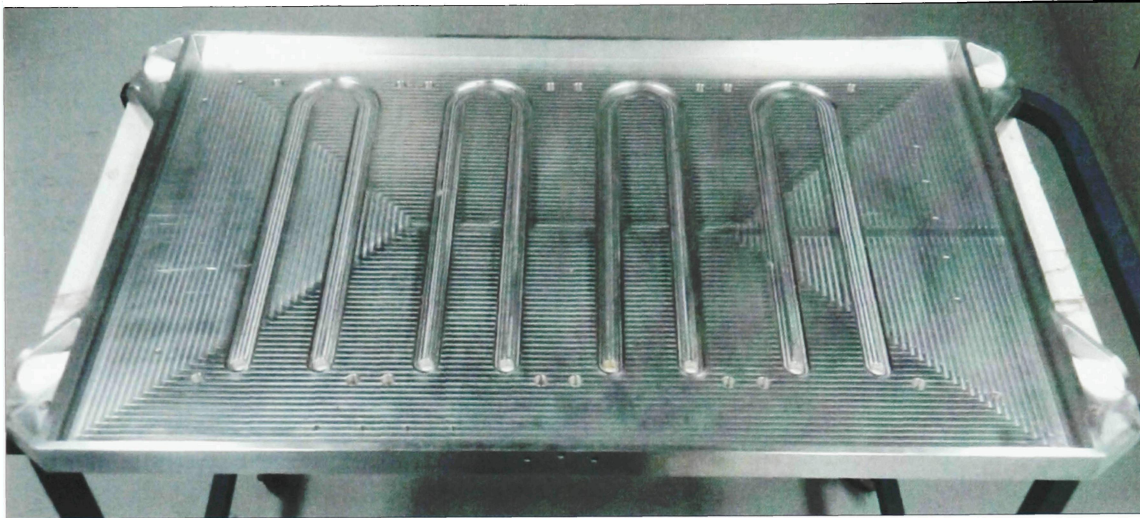


Figure 40: Finished Structural Cold Plate

Plastic mock-ups of the A123® 25S2P modules have been created (Figure 41) to allow the EcoEagles to pre-assemble all other components of the ESS without the danger of electric shock.



Figure 41: Finished Structural Cold Plate with A123® 25S2P Module Mock Ups

A CAD rendering of the final ESS assembly can be seen in Figure 42.

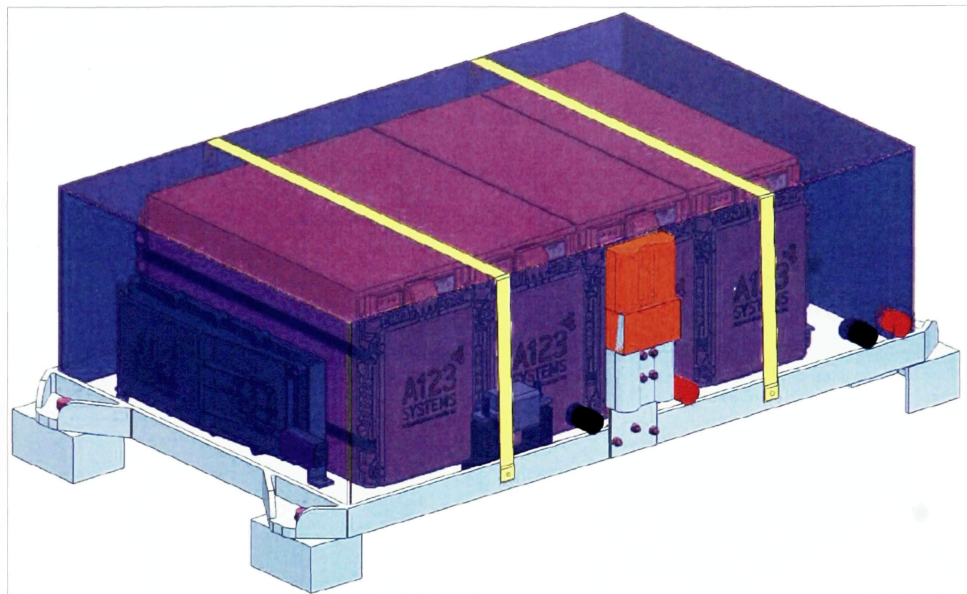


Figure 42: ESS Assembly (26)

Figure 43 shows the location of the battery pack in relation to the rear crush zone. The pack is bolted to the rear frame rails of the Vue through elastomeric vibration isolators.

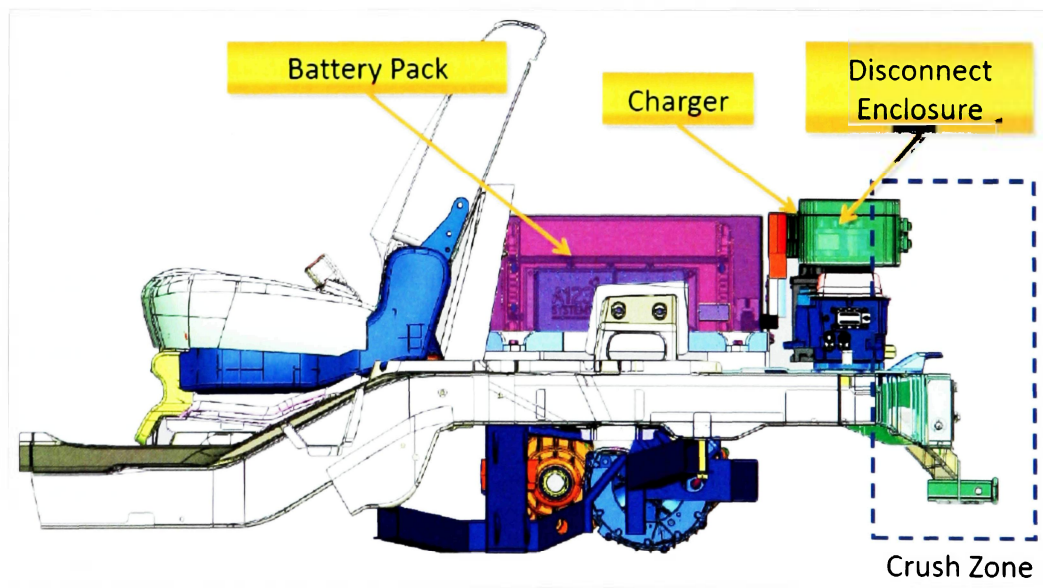


Figure 43: Battery Pack Location Outside of Rear Crush Zone (26)

The major dimension of the ESS can be seen in Figure 44.

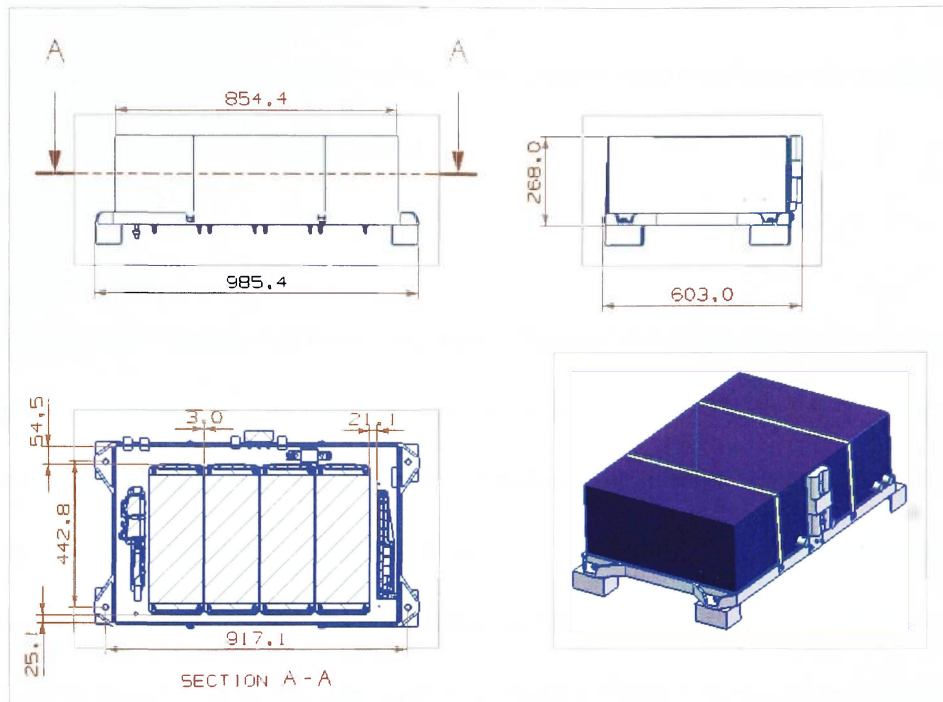


Figure 44: Major Dimensions of ESS in mm (26)

System Limitations

The system is capable of maintaining safe and uniform battery temperature at ambient temperatures up to 40 °C and 66.7 A_{RMS} . If the ambient temperature and/or current rises above the previously noted values there is a potential for the batteries to reach an unsafe temperature. Since either of these two events are likely to occur, it becomes necessary to implement a control strategy in vehicle's control system that regulates the available current as a function of ESS temperature. Such a control strategy would prevent a catastrophic battery failure in extreme operating conditions.

CHAPTER 5: RECOMMENDATIONS

Throughout the course of this study, several observations were made that could be extremely beneficial to the future study of this subject. This chapter discusses these observations as well as suggestions for a more in-depth analysis.

Analysis Limitations

The analysis in this research was limited by several factors relating to computational capabilities and available information. The computations were limited by the amount of Random Access Memory available (RAM). The computer used for the analysis had 6 GB of RAM available. The operating system and background tasks left 5 GB of the 6 GB for use by the Flow Simulation software. For intricate analyses, the computational time increased exponentially once the RAM reached 100% usage. Therefore, the models were simplified, in terms of both geometry and mesh refinement, so that the simulation did not utilize all of the available RAM. Currently there are computers available with >16 GB of ram, however, the budget of this study does not permit such a platform to be acquired (48).

The lack of data available from manufactures of heat exchangers also presented a problem when selecting a heat exchanger for the thermal management system. A large majority of the suppliers of heat exchangers target automotive enthusiasts. These enthusiasts tend to put forth very little engineering analysis in the selection of a heat exchanger for their application. Therefore, the market is saturated with qualitative descriptions of products rather than useful quantitative data. This forces one to perform additional analysis to determine the performance of the heat exchanger. The thin walls and intricate geometry make such an analysis difficult and force the designer to make significant assumptions and simplifications to reach a feasible analysis.

Future Research: Time Dependent Analysis

The analysis presented in the previous chapters represents a steady state case at a constant ambient temperature and a constant current. It may be beneficial to perform an analysis where the current and therefore ohmic heat production is time dependent. This could be done using data from the PSAT simulation mentioned in chapter 2. The results of the simulation would yield information on duty cycle durations for which the ESS can operate above the RMS towing current without overheating.

Future Research: Heat Soaked ESS

The ESS is located in the rear of the vehicle compartment underneath a removable floor. Since the battery is in a closed space, the lack of air circulation may present heating problems on hot/sunny days if the vehicle is parked outside. Some solutions to this potential problem may be tinting the windows of the vehicle to prevent a greenhouse effect, running the thermal management system before drawing current from the ESS, or providing ventilation to the ESS compartment.

REFERENCES

1. **Chagnon, Guy.** *High Power Lithium-Ion for Hybrid Electric Vehicles.* s.l. : SAE International, 1998. 981251.
2. **Naoki Amada, Masato Fukino, Masahiko Tahara, Tadaaki Liyama.** *Development of a Performance Prediction Program for EVs Powered by Lithium-Ion Batteries.* s.l. : SAE International, 1997. 970239.
3. **Christian St-Pierre, Roger Rouillard, Andre Belanger, Bruno Kapfer, Martin Simoneau, Yves Choquette, Louis Gastonguay.** *Lithium Polymer Battery for EVs and HEVs.* s.l. : SAE International, 2000. 2000-01-1587.
4. **Thomas Sack, Michael Saft, Guy Chagnon, Salah Oweis, Antonio Romero, Michael Zuhowski, Thierry Faugas, Guy Sarre, Pierre Morhet, Louis d'Ussel.** *Lithium Ion Energy and Power Storage Technology.* s.l. : SAE International, 2000. 2000-01-1589.
5. **Raymond Hobbs, Donald Karner, Frank Flemming, Russell Newnham.** *Development of Optimized Fast Charge Algorithms for Lead Acid Batteries.* s.l. : SAE International, 1999. 1999-01-1157.
6. **Masato Origuchi, Takeshi Miyamoto, Hideaki Horie, Kiyoshi Katayama.** *Development of a Lithium-Ion Battery System for EVs.* s.l. : SAE International, 1997. 970238.
7. **BOSCH.** *Automotive Handbook: 6th Edition.* Postfach : Robert Bosch GmbH, 2004. ISBN: 0-7680-1513-8.
8. *What Are Batteries, Fuel Cells, and Supercapacitors?* **Martin Winter, Ralph Brodd.** 104, s.l. : American Chemical Society, 2003.
9. **G. Fritz, N. Karditsas, S. Venkatesan, D. Corrigan, S. K. Dhar, S. R. Ovshinsky.** *Ovonic NiMH Batteries: The Enabling Technology for Heavy-Duty Electirc & Hybrid Electric Vehicles.* s.l. : SAE International, 2000. 2000-01-3108.
10. **Sandeep Dhameja, Min Sway-Tin.** *Traction Batteries Their Effects on Electric Vehicle Performance.* s.l. : SAE International, 1997. 970240.
11. **Takeshi Miyamoto, Etsuo Oogami, Masato Origuchi, Tadashi Tsuji, Norihiko Hirata, Tatsuo Horiba.** *Development of a Lithium-Ion Battery System for HEVs.* s.l. : SAE International, 2000. 2000-01-1057.
12. **Dwaine Coates, Allen Charkey.** *Nickel-Zinc Batteries for Commercial Applications.* s.l. : SAE International, 1999. 1999-01-2512.

13. **Chris Mi, Ben Li, Derrick Buck, Naoki Ota.** *Advanced Electro-Thermal Modeling of Lithium-Ion Battery System for Hybrid Electric Vehicle Applications.* s.l. : IEEE, 2007. 0-7803-9761-4/07.
14. **EcoEagles.** *Design Overview of the Embry-Riddle HyREV Propulsion System: Report 5.* [Document] Daytona Beach : Embry-Riddle Aeronautical University, 2009.
15. 09May14_090514004.jpg. *EcoCar Challenge.* [Online] [Cited: November 6, 2009.] http://pa.photoshelter.com/c/ecocarphoto/gallery-img-show/EcoCar/G0000M.rw5TAzkqo/?&_bqG=1&_bqH=eJyLLE7MKM12dHIJzHbT9XCucvSqNA7OdDFP9Cq3MrYyMrWyco_3dLF1NwACX72ictMQx6rswny1AJComrtvLujj49rUCQ2RQAYUhvU&I_ID=I0000kK69BEWb7s4.
16. EcoCAR_Fall Workshop .09. *EcoCAR Challenge.* [Online] [Cited: November 6, 2009.] http://pa.photoshelter.com/c/ecocarphoto/gallery-img-show/Boston-Fall-09/G0000tcN7gg7BfQI/?&_bqG=0&_bqH=eJwzD8vOqcrJCokISStNc68s93SMqtINjTIsScq3MjQwtDlytbJyj_d0sXU3AIKSZD_z9HRzp7RAT7UAkKiau2e8u6OPj2tQJDZFAH1KHG8-&I_ID=I0000Lt4KUrDqI7I.
17. **A123 Systems.** *Prismatic Module Thermal Analysis Guidelines.* [Document] 2009.
18. —. [Online] <http://www.a123systems.com/cms/product/image/7/medium/A123-017.jpg>.
19. —. *Introducing a New Module for The EcoCAR Battery Packs.* [Power Point Presentation] 2009.
20. **Massachusetts Institute of Technology.** Thermal Resistance Circuits. [Online] [Cited: June 6, 2009.] <http://web.mit.edu/16.unified/www/SPRING/propulsion/notes/node118.html>.
21. **EcoEagles.** *Brusa Charger Equiped.* [JPEG Image] Daytona Beach : Embry-Riddle Aeronautical University, 2009.
22. —. *A123 Battery Pack Design: CAD Design Review.* [Power Point Presentation] Daytona Beach : Embry-Riddle Aeronautical University, 2009.
23. Properties of Aluminum Alloy AA 6061. *Efunda.* [Online] [Cited: November 6, 2009.] http://www.efunda.com/materials/alloys/aluminum/show_aluminum6061.html.
24. Table of Specific Heats. *Hyperphysics.* [Online] [Cited: November 6, 2009.] <http://hyperphysics.phy-astr.gsu.edu/HBASE/Tables/sphtt.html>.
25. **U.S. Department of Energy.** Argonne PSAT Model. *Argonne National Laboratory.* [Online] [Cited: October 23, 2009.] http://www.transportation.anl.gov/modeling_simulation/PSAT/index.html.

26. **EcoEagles.** *A123 Design Review.* Daytona Beach : Embry-Riddle Aeronautical University, 2009.
27. Emissions Test Cycles: FTP-72 (UDDS). *DieselNet: Diesel Emissions Online.* [Online] [Cited: November 8, 2009.] <http://www.dieselnet.com/standards/cycles/ftp72.html>.
28. Emission Test Cycles: EPA Highway Fuel Economy Cycle. *DieselNet: Diesel Emissions Online.* [Online] [Cited: November 8, 2009.] <http://www.dieselnet.com/standards/cycles/hwfet.html>.
29. **Ahmad Pesaran, Andreas Vlahinos, Steven Burch.** *Thermal Performance of EV and HEV Battery Modules and Packs.* Golden, Colorado : National Renewable Energy Laboratory.
30. **Dassault Systèmes.** *SolidWorks Flow Simulation 2009: Technical Reference.* [Document]
31. —. SolidWorks CFD Flow Simulation. *SoildWorks.* [Online] [Cited: August 11, 2009.] <http://www.solidworks.com/sw/products/cfd-flow-analysis-software.htm>.
32. **National Aeronautics and Space Administration.** Navier-Stokes Equations. *The National Aeronautics and Space Administration.* [Online] [Cited: October 24, 2009.] <http://www.grc.nasa.gov/WWW/K-12/airplane/nseqs.html>.
33. **Dassault Systèmes.** *SolidWorks Flow Simulation 2009: Tutorial.* [Document]
34. Aluminum Thermal Properties. *The Engineering Toolbox.* [Online] [Cited: November 6, 2009.] <http://www.engineeringtoolbox.com>.
35. Water - Thermal Properties. *The Engineering Toolbox.* [Online] [Cited: November 6, 2009.] <http://www.engineeringtoolbox.com>.
36. **RSS Weather.** World Weather Forecasts by RSS. *Climate in Yuma, Arizona.* [Online] [Cited: November 8, 2009.] <http://www.rssweather.com/climate/Arizona/Yuma/>.
37. **The Engineering ToolBox.** Ethylene Glycol Heat-Transfer Fluid. *The Engineering ToolBox.* [Online] September 12, 2008. [Cited: October 22, 2009.] http://www.engineeringtoolbox.com/ethylene-glycol-d_146.html.
38. **CBS Interactive Inc.** HP Pavilion-dv7-1285dx. *CNET Reviews.* [Online] March 25, 2009. [Cited: November 24, 2009.] http://reviews.cnet.com/laptops/hp-pavilion-dv7-1285dx/4505-3121_7-33496197.html.
39. **Dessault Systèmes.** *SolidWorks Flow Simulation 2009: Solving Engineering Problems.* [Document]
40. **EcoEagles.** *System Development and Integration: Report 4.* [Document] Daytona Beach : Embry-Riddle Aeronautical University, 2009.

41. **Summit Racing Equipment.** Fluidyne High Performance DB30618 Fluidyne Fluid Coolers Overview. *Summit Racing High Performance Car and Truck Parts*. [Online] [Cited: July 21, 2009.] <http://www.summitracing.com/parts/FLD-DB30618/?image=large>.
42. **Spal Automotive.** Motorcycle/ATV: 30103084. *SPAL USA*. [Online] [Cited: August 10, 2009.] <http://www.spalusa.com/store/main.aspx?p=itemdetail&item=30103084>.
43. **Yunus Cengel, John Cimbala.** *Fluid Mechanics: Fundamentals and Applications*. New York : McGraw-Hill, 2006. ISBN 0-07-247236-7.
44. **Fluidyne.** Therm-Hx Engine Oil Coolers. *Fluidyne High performance Radiators and Oil Coolers*. [Online] [Cited: October 26, 2009.] http://www.fluidyne.com/pl_theoc.html.
45. **Summit Racing Equipment.** Dedenbear WP3 - Dedenbear Remote Water Pumps - Overview. *Summit Racing High Performance Car and Truck Parts*. [Online] [Cited: July 21, 2009.] <http://www.summitracing.com/parts/DED-WP3/?image=large>.
46. *Battery Thermal Management System Design Modeling*. **G.H. Kim, A. Pesaran**. Yokohama : National Renewable Energy Laboratory, 2009. NREL/CP-540-40446.
47. **Lytron Inc.** Lytron Thermal Reference. *Lytron Total Thermal Solutions*. [Online] [Cited: October 28, 2009.] <http://www.lytron.com/tools-technical/thermal-reference/temperature-change-graphs.aspx>.
48. **UpgradeComputerMemory.** HP Workstation xw9300. *Upgrade Computer Memory*. [Online] [Cited: October 23, 2009.] <http://www.upgradecomputermemory.com>.

